DOE/ER/12120--T1

SRL- 8-F-1996

THE PLASMA CENTRIFUGE
A Compact, Low Cost, Stable Isotope Separator

Prepared by

Dr. William Guss

SCIENCE RESEARCH LABORATORY, INC.
15 Ward Street
Somerville, MA 02143

September 5, 1996

PHASE II FINAL TECHNICAL REPORT

Period for September 15, 1991 to September 14, 1995

Contract No. DEFG02-91ER12120

Prepared for

DEPARTMENT OF ENERGY
9800 South Cass Avenue
Argonne, IL 60439

DISCLAIMER

TABLE OF CONTENTS

Abstract

Enriched stable isotopes are required for production of radionuclides as well as for research and diagnostic uses. Science Research Laboratory (SRL) has developed a plasma centrifuge for moderate throughput of enriched stable isotopes, such as ^{13}C, ^{17}O, ^{18}O, and ^{203}Tl, for medical as well as other applications. Dwindling isotope stocks have restricted the use of enriched isotopes and their associated labelled organic molecules in medical imaging to very few research facilities because of high costs of isotope separation. With the introduction of the plasma centrifuge separator, the cost per separated gram of even rarely occurring isotopes ($\leq 1\%$ natural abundance) is potentially many times lower than with other separation technologies (cryogenic distillation and calutrons). The centrifuge is a simple, robust, pulsed electrical discharge device that has successfully demonstrated isotope separation of small (mg) quantities of ^{26}Mg. Based on the results of the Phase II program, modest enhancements to the power supplies and cooling systems, a centrifuge separator will have high repetition rate (60 pps) and high duty cycle (60%) to produce in one month kilogram quantities of highly enriched stable isotopes. The centrifuge may be used in stand-alone operation or could be used as a high-throughput pre-separation stage with calutrons providing the final separation.

A. INTRODUCTION

Nuclear medicine has evolved rapidly and continuously since the WWII days when the Manhattan Project and then the Atomic Energy Commission (AEC) first provided the medical community with radioactive isotopes at low cost. The calutrons (California University cyclotrons) at Oak Ridge National Laboratory (ORNL) were an important source of separated materials for the war effort, and thereafter provided the material needed for the development of peaceful uses of atomic energy for medicine. ORNL produced material for its own requirements as well as fulfilling the needs of the other National Laboratories, and for industrial (commercial) and research purposes. However the main emphasis of the ORNL facility remained the separation of uranium isotopes for weapons and nuclear fuel. The facilities have aged becoming less cost effective and are now maintained in standby mode. The result has been that the U.S. has now come to rely on foreign suppliers for an increasing fraction of the precursor materials and final products.

In recent years, the problem has become acute on at least one occasion when the U.S. supply of technetium (from molybdenum generators) from Canada was compromised and various groups, including the Society of Nuclear Medicine and the American College of Nuclear Physicians, called attention to the major problem that would occur in the health care system if supplies of these stable medical isotopes were interrupted for any period of time. Reliability of the isotope supply has improved somewhat with another source of stable isotopes and radionuclides having recently appeared. With the cessation of the Cold War, the former Soviet Union has started to sell some of its stockpile of isotopes as it has entered the world economic community. At this time, the reliability and cost of this source is difficult to assess. Budding entrepreneurship in the former Soviet Union has propelled prices upwards in other markets and isotope prices will probably follow. In addition, there may be breakdowns in the distribution system between Russia and the former Soviet Republics.

Radionuclides are produced in large high flux reactors (neutron excess nuclides) and charged-particle accelerators (proton excess nuclides). Some of the materials come from industry, some from National Laboratories (U.S. and elsewhere), and some from university facilities having cyclotrons and the newly emerging linear accelerators designed for isotope production. In addition, dedicated facilities for large scale production of research material are being proposed, *viz.* Brookhaven National Laboratory (upgrade at the Brookhaven Linear Isotope Producer (BLIP)), Texas (facility redesign at SSC), and proposals are being processed for a National Biomedical

Tracer Facility (NBTF). All of these resources rely upon the availability of the high purity target materials needed for the particular reactors that are used to produce the radionuclides needed for medical use. The parent materials for these required isotopes can be solids, liquids or gases. Some use high purity, naturally-occurring materials, and others require a high degree of enrichment of particular isotopes of the elements to be activated. It is this task that the calutrons performed, and which is still needed today.

Over the last decade or two, the Department of Energy has sponsored the development of several advanced separation technologies such as the atomic vapor laser isotope separation (AVLIS), and the Gas Centrifuge. These technologies are capital intensive and designed for optimal outputs of $100 - 1000\,kg/y$, of a very few isotopes in the nuclear fuel cycle. Much smaller quantities ($\approx 0.1 - 1\,kg/y$) of other isotopes are used as parents for radioactive isotopes used in nuclear medicine.[1] About 30 different isotopes[2] varying in mass from ^{13}C to ^{203}Tl are regularly used in biomedical research and clinical practice for myocardial studies, for positron emission tomography (PET), for magnetic resonance imaging (MRI), and as metabolic tracers in the human body. A still wider variety of isotopes in even smaller quantities ($\approx 1 - 10\,g/y$) is used for research in nuclear physics and chemistry[3] as targets for the production of ion beams of exotic nuclei. Recently, the cryogenic distillation process (ICONS) developed[4] at Los Alamos National Laboratory (LANL) has entered the commercial sector for the production of enriched isotopes of C, N, O, and S. Also, the liquid/gaseous thermal diffusion process developed at Mound Laboratories has been used to enrich mostly deuterium and noble gases. Because of the high temperatures required, very few metals are enriched by this diffusion process.

The uses for these isotopes are varied and numerous and find applications not only in medical imaging but other areas as well. Isotopes have been used or are proposed for use in such areas[5] as Food and Agriculture, Biochemistry, Nuclear Fusion, Cosmology, Earth Sciences, Ecology, Health Care, Nutrition, Toxicology, and Materials Science.

A particular advantage of stable isotopes as tracers in biomedical and clinical studies is that they can be administered to humans without concern for radiation or toxic side effects. They are also of special use in the determination of biological structures due to their detectability by a variety of methods. Specifically, ^{13}C, ^{17}O, and ^{15}N are rare stable isotopes that are observable by nuclear magnetic resonance techniques, and this, together with site-specific labelling, has led to the concept of "stable-isotope assisted structure determination". In the last decade there has been a

dramatic growth in the application of MRI techniques to the study of living systems. Starting from the study of cells and tissue cultures *in vitro*, MRI is today applied to studies of intact animals and humans. MRI has been a technique of interest to physicists and has been a tool for chemists and biochemists since the 1940s. With the advent of improved high-field magnets with warm-bore dimensions large enough to accept humans, coupled with the development of Fourier transform imaging techniques permit localization of MRI spectra to volumes as small as $1\ cm^3$ located deep in the interior of the human body. This ability has transformed MRI into a technique that not only provides morphological information but also into a metabolic probe. Today MRI techniques rival or sometimes surpass other existing imaging modalities such as x-rays and computed tomography in their ability to provide anatomic detail. The improved image contrast between soft and hard tissue, and the potential for using MRI for quantitative tissue characterization to distinguish different pathologies, monitor metabolic changes, and provide functional maps of image function, makes it one of the most attractive diagnostic imaging tools. Unfortunately one of the current limitations of MRI is the expense and cost of the entire procedure, particularly the contrast materials and metabolic labels.

Stable isotopes are important to imaging techniques other than MRI. The characteristics and benefits of MRI not withstanding, other techniques have distinct advantages for particular studies. The two photon annihilation radiation in PET resulting from positrons interacting with nearby electrons has been found not only to present less of a radiation burden on the subject than conventional gamma-ray techniques, it offers tomographic imaging advantages unmatched by single photon techniques. This technique is has been found to be very useful as a probe of physiological processes essential to life that are unavailable by any other technology. In contrast to MRI which utilizes stable isotopes, PET commonly uses the short-lived, positron emitting radionuclides, ^{11}C, ^{13}N, ^{15}O, and ^{18}F. These isotopes are derived from stable ^{11}B, ^{13}C, ^{15}N, and ^{18}O which have naturally occurring abundances of 80.1%, 1.1%, 0.37%, and 0.20% respectively. Because the half lives of the positron emitters can be short, ranging from minutes to 100 minutes, a source for their generation is required in the immediate vicinity of their end use. Typically medical and research facilities have their own dedicated cyclotrons or electrostatic accelerators that produce high energy ($6 - 9\,MeV$ deuteron, $10 - 18\,MeV$ proton), low current ($\approx 50\mu A - 1\,mA$) beams required to produce up to several Curies per day of the unstable isotopes.

The most common radionuclide used in nuclear medicine imaging is ^{99m}Tc (half-life

six hours) and accounts for 80% of all nuclear medicine procedures. Technetium is not found in nature and must be generated from the unstable isotope ^{99}Mo which in turn must itself be artificially produced either by neutron activation of stable ^{98}Mo (24.1%) or by collection from fission products. Incorporated into chemical compounds, ^{99m}Tc accumulates in various target organs such as the heart, kidneys, thyroid, and lungs and emits γ rays which have sufficient energy that they have minimal interaction with surrounding tissue. As a result, very small amounts are needed for diagnostic images with the added benefit that chemical poisoning and radiation damage are not problematic.

With the increased interest in metabolism, in humans and other animals, other elements and isotopes are also in demand. Certain dietary studies of trace metals involving the elements selenium, molybdenum, copper, and rubidium require a supply of enriched isotopes. Another area of recent interest is the study of osteoporosis, investigations of which require isotopes of calcium, ^{42}Ca (0.65%) and ^{44}Ca (2.1%). In addition to osteoporosis, bone formation and loss have also been found to be important for humans during space flights.

In materials science, isotopes serve some of the same uses as in the biological and medical sciences. Isotopes can be introduced into a material as a tracer. With larger quantities of an isotope it is possible to isotopically tailor materials. It has been proposed[6] that steels and inconels in high density neutron environments (fission and fusion reactors) be made with nickel ^{58}Ni (68.1%) and molybdenum ^{96}Mo (16.7%) isotopes with small neutron cross sections to reduce the resulting radioactive-waste management problem. For naturally occurring gadolinium (7 stable isotopes), the thermal neutron cross section is $4.9\times10^4\,b$. Gadolinium has two isotopes with very large thermal neutron cross sections. ^{157}Ga (15.65%, $2.54\times10^5\,b$), largest known of any element) and ^{155}Ga (14.8%, $6.1\times10^4\,b$) which are useful as compact neutron absorbers and control rods in fast reactors. An isotope of boron, ^{10}B (19.6%), also has a large neutron absorption cross section ($3.84\times10^3\,b$ and has found similar applications. Isotopic refining would reduce the amount of boron and gadolinium required for a specific application.

We have summarized above the current situation and a much more detailed description of the isotope supply and production capability is contained in a recent report from the Institute of Medicine of the National Academy of Sciences[7].

And while other plasma-based isotope separation equipment (Plasma Separation Process

- PSP) is located at ORNL, the plasma centrifuge offers significant advantages. In scale, the prototype PSP superconducting magnet is large, $8\,m$ long with a $1\,m$ bore and magnetic fields of $2-6\,T$, The existing centrifuge device comparable in mission and capability to the PSP device and is $1.5\,m$ long with a $0.2\,m$ bore and magnetic fields of $0.1-0.2\,T$. The centrifuge is also more energy efficient (Table I) producing plasma with temperature of a few eV as opposed to the PSP plasma ion temperature of keV.

Table I
Separator Comparisons for Various Isotopes
(Energy Required per Separated Atom)

Process	^{50}V	^{77}Se	^{203}Tl
Calutron	$3.3\,GeV$	$\approx 2\,GeV$	$\approx 2\,GeV$
PSP (TRW)	$200\,keV$		
Gas Centrifuge	$20\,keV$	no source	no source
AVLIS	$10-20\,keV$	$\approx 10\,keV$	$\approx 10\,keV$
Plasma Centrifuge	$280\,keV$	$8.9\,keV$	$2.3\,keV$

Science Research Laboratory has developed the vacuum-arc centrifuge (VAC) and constructed a proof-of-principle device for the enrichment of stable isotopes. The vacuum-arc centrifuge and its developmental history are presented in the following section. The vacuum-arc refers to the source type and the centrifuge action results from the rotating plasma column created by the source. Here we describe how it is possible to produce various enriched isotopes in the quantities and purities needed to sustain the growing medical as well as other applications in U.S. and elsewhere, and to complement and ultimately replace the older calutron technology.

B. BACKGROUND, TECHNICAL APPROACH AND RESULTS

B.1 Prior Plasma Centrifuge Research

The U.S. Government has in the past supported several different methods of isotope separation. While the primary material processed was uranium, many other isotopes were also processed. Traditional methods include gaseous diffusion, gas centrifuges, and calutrons (basically a mass spectrograph). Several advanced separation methods[8] have been developed including AVLIS and two plasma based techniques, the plasma centrifuge and another based on ion cyclotron resonance heating. The Department of Energy facility at Oak Ridge, Tennessee housed most of the traditional processing equipment, and much of the separation work there has ceased, although there are plans

to revive the calutrons.

The gaseous centrifuge operates by spinning a large cylinder filled with a gas containing the element to be separated. In this concept, the centrifugal force which is proportional to the square of the rotational velocity, causes the mass separation. For most efficient separation high rotational speeds are required but these speeds are limited to the speed of sound, about $3 \times 10^3\, rad/s$ $(30,000\, rpm)$. In addition to the acoustic limit, strength of materials considerations and precision machining practice are are also factors in this limit. The enrichment per pass through the centrifuge was about 0.8%.

Utilizing plasmas rotating in a magnetic field eliminates acoustic, materials and machining constraints and lead to the concept of the plasma centrifuge. Centrifugal isotope separation in rotating plasmas has been studied for over three decades. Following early work by Slepian[9] and Bonnevier[10], later researchers[11–15] have measured isotopic enrichment in gaseous, rotating plasmas. Typical enrichments[13] of $\sim$10% in ^{22}Ne were reported. In the decade of the seventies, a considerable body of scientific literature was accumulated with regard to rotation rates and measured element and isotope separation in a variety of gas discharge plasmas. Contributions to this field were made by research groups in Britain, Sweden, Germany, Netherlands and Australia. In spite of the diversity of research worldwide, progress in the field, as evidenced by higher enrichments or practical embodiments of the research devices, was hampered by the deleterious effects of the ever present neutral atoms in these centrifuges. A notable research effort in Australia[13–15] indicated the difficulty of improving the partially ionized centrifuge any further. The problem arises because the remaining neutral atoms do not feel the Lorentz force, and their drag on the ions limits the rotation velocity of the ions.

With the development at Yale in 1980 of the vacuum-arc centrifuge[16] a fully ionized plasma source was realized. In the Yale device, as in the SRL device, an arc is struck between a cathode biased negatively by a capacitor bank, on the axis of the axial magnetic field, and a grounded anode made of a semi-transparent metal screen. Even with its improved ionization fraction, separations in the Yale experiment were still only modest.

Analytic work[17] suggested that for a plasma flowing along an axial magnetic field and creating a radial space charge electric field, two distinct equilibria could exist. The main feature that distinguished these equilibria was the frequency of plasma rotation. The difference in rotation

frequency, for the parameters of the Yale experiment, could be a factor-of-ten. Probe and spectroscopic measurements of the Yale plasma suggested that the rotation frequency was $2 \times 10^5\, rad/s$ ($2 \times 10^6\, rpm$), which corresponded to the lower of the two rotational frequencies.

In 1989, a group at Ibaraki University in Japan demonstrated[18] for the first time a much higher plasma rotation frequency ($2 \times 10^6\, rad/s$ or $2 \times 10^7\, rpm$) which corresponded to the higher rotational equilibrium. As part of this Phase II program, SRL staff members traveled to Tokyo, Japan to attend the Twelfth International Conference on Electromagnetic Isotope Separators and to visit the Ibaraki device. Under the guidance of some of the Yale group who had joined SRL, a vacuum arc centrifuge was proposed and constructed which also demonstrated the higher plasma rotation. Table II compares the various centrifuge results and shows the advantages of the plasma centrifuge.

Table II
Separative Power Comparison for Gas and Plasma Centrifuges
ΔM=2 amu, r_p=5 cm

	Gas Centrifuge	Yale Centrifuge	Ibaraki Centrifuge	SRL Centrifuge
$\omega\ (rad/s)$	3×10^3 ($3 \times 10^4\, rpm$)	2×10^5 ($2 \times 10^6\, rpm$)	1.1×10^6 ($1 \times 10^7\, rpm$)	1.6×10^6 ($1.5 \times 10^7\, rpm$)
T_e (eV)	0.03	2	10	$\approx$8
Separation Factor (α)	8×10^{-3}	0.19	1.14	3
Enrichment per Pass (%)	0.8	68	221	1940

Figure 1 illustrates the centrifuge geometry. The source consists of a cathode of the desired element and a mesh anode. A pulse forming network (PFN) provides a low voltage ($-100\, V$), high current ($3\, kA$) pulse of length $10\, ms$. A laser focused on the cathode creates a localized arc which initiates the discharge. An approximately uniform axial magnetic field extends from the cathode region beyond the anode to the collection area which is approximately $1\, m$ from the cathode. At the collection area, an arm intercepts the outer edge of the plasma where the enriched isotope is localized.

The plasma source for the centrifuge in general works very well and has a very high electrical efficiency for coupling energy into the cathode to produce the plasma. The plasma transport efficiency through the anode mesh could be improved. In the present design, the anode mesh is approximately 50% transparent and, under the heat load of the intercepted plasma, is prone

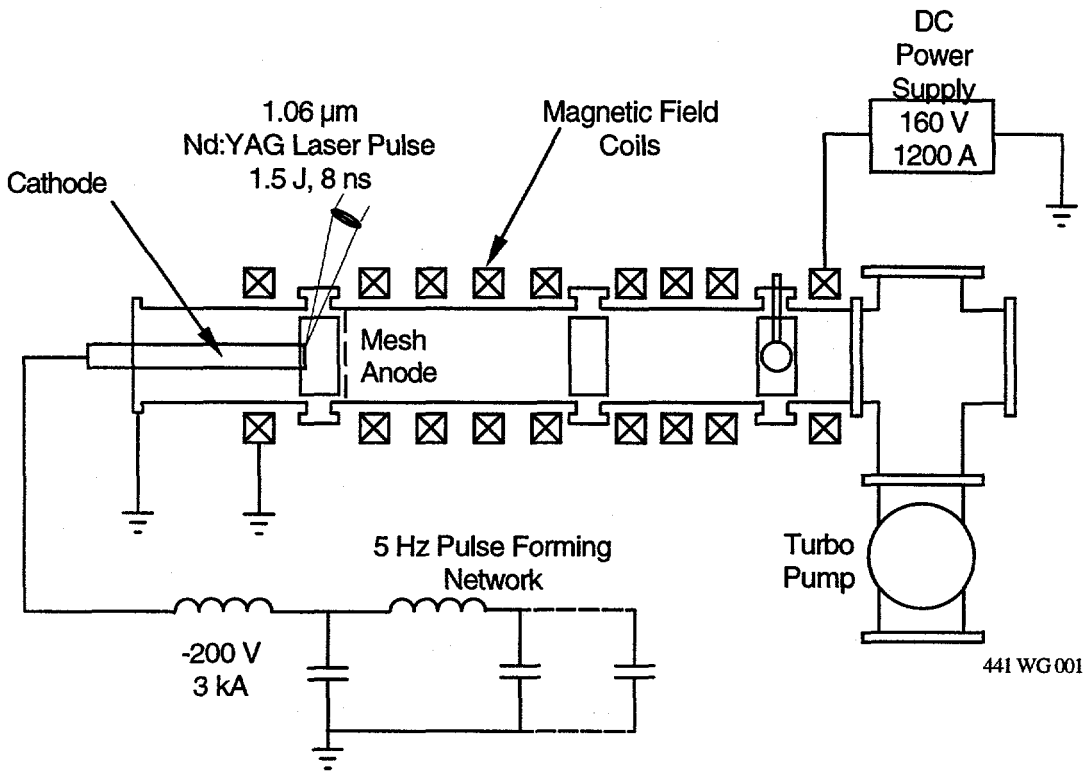

Figure 1: SRL Plasma Centrifuge Schematic.

to failure. We anticipate that a more robust source would be required for prolonged operation with large quantity collections.

Through the efforts of a number of different groups, the plasma centrifuge has been well characterized. Results of the SRL centrifuge will be presented following the physics model for the centrifuge below.

B.2 Physics Characterization

In this section the principles governing the separation process and the plasma equilibria are presented. The fluid analysis of the gaseous centrifuge follows a similar set of equations.

The centrifuge plasma can be modeled as an infinite cylinder of fully ionized, magnetized plasma in which axial and azimuthal gradients and viscous effects are ignored. Experiments[19,20] have shown that there is minimal z dependence of plasma parameters in the column ($i.e.$ there is no change in the column with axial distance from the source region) and that it is axisymmetric. It is thus appropriate to use cylindrical coordinates and to neglect the axial and azimuthal gradients. A reasonably complete description of the plasma dynamics is obtained from a two-fluid model

which treats the ions and electrons as co-moving fluids. The variables of interest are the density n, velocity v and pressure P of each species s. For a cylindrical geometry in which collisions are neglected and thus no radial diffusion occurs, a description of each of the fluids is given by the continuity equation,

$$\frac{\partial n_s}{\partial t} + \nabla \cdot (n_s \vec{v}_s) = 0 \tag{1}$$

the momentum equation,

$$n_s m_s \frac{\partial \vec{v}_s}{\partial t} + n_s m_s (\vec{v}_s \cdot \nabla) \vec{v}_s = -\nabla P_s + q_s n_s \left(\vec{E} + \vec{v}_s \times \vec{B} \right) \tag{2}$$

and Maxwell's equations,

$$\epsilon_o \nabla \cdot \vec{E} = \rho$$

$$\nabla \times \vec{B} = \mu_o \vec{J} + \frac{1}{c^2} \frac{\partial \vec{E}}{\partial t}$$

$$\nabla \times \vec{E} + \frac{\partial \vec{B}}{\partial t} = 0$$

$$\nabla \cdot \vec{B} = 0$$

where the total charge density is

$$\rho = \sum_s q_s n_s$$

and the total current density is

$$\vec{J} = \sum_s q_s n_s \vec{v}_s$$

where m_s and q_s are the mass and charge of the species s. Steady state is assumed, thus reducing to zero all time derivatives. The radial component of the momentum equation (Eqn. (2)) reduces to:

$$n_s m_s v_{sr} \frac{\partial v_{sr}}{\partial r} - n_s m_s \frac{v_{s\theta}^2}{r} = -\frac{\partial p_s}{\partial r} + q_s (E_r + v_{s\theta} B) \ . \tag{3}$$

Again experiments have shown[19,20] that the size of the column does not change appreciably with axial distance. Consequently the radial velocity can be assumed to be small. The azimuthal components of the momentum equations of the electrons and the i^{th} ion species are then:

$$-n_e m_e \omega_e^2 r = -\frac{dp_e}{dr} - n_e e (E_r + \omega_e r B) \tag{4}$$

$$-n_i M_i \omega_i^2 r = -\frac{dp_i}{dr} + n_i Z_i e (E_r + \omega_i r B) \tag{5}$$

where ω_e and ω_i are the rigid-rotor frequencies of the electrons and ions respectively. The omission of collisional momentum exchange terms from the above equations is justified because the transit

time of plasma through the centrifuge is short and no appreciable collisional diffusion occurs. If the plasma ions are assumed isothermal and the scalar ion pressures are expressed by an equation of state as $p_i = n_i kT_i$, where k is Boltzmann's constant. Making the pressure terms the subjects of Eqns. (4) and (5), integrating between r=0 and some radius r yields for the i^{th} species:

$$n_i(r) = n_i(0) \exp\left[\frac{e}{kT_i}\left(-Z_i\phi(r) + \frac{\omega_i Z_i B r^2}{2} + \frac{M_i\omega_i^2 r^2}{2e}\right)\right] . \tag{6}$$

It is possible to determine the separation of different isotopes using the density profiles of each of the ion species. The relative abundance, also called the abundance ratio R, of two different ion species with masses M_1 and M_2 and charges Z_1 and Z_2 at a distance r from the column axis is given by

$$\begin{aligned} R(r) &= \frac{n_2^{Z_2}(r)}{n_1^{Z_1}(r)} \\ &= R(0) \exp\left[-\frac{(Z_2 - Z_1)e}{kT_i}\left(\phi(r) + \frac{\omega r^2 B}{2}\right) + (M_2 - M_1)\frac{\omega^2 r^2}{2kT_i}\right] . \end{aligned} \tag{7}$$

For the special case that $Z_1 = Z_2$, the simpler result is

$$R(r) = R(0) \exp\left[\frac{(M_2 - M_1)\omega^2 r^2}{2kT_i}\right] . \tag{8}$$

From the above, the normalized abundance ratio $R(r)/R(0)$ or enrichment factor can be defined as

$$\begin{aligned} \gamma &= R(r)/R(0) \\ &= \exp\left[\frac{(M_2 - M_1)\omega^2 r^2}{2kT_i}\right] . \end{aligned} \tag{9}$$

The coefficient of r^2 within the exponential argument in the above equations is the separation factor α of the vacuum-arc centrifuge, given by

$$\alpha = \frac{(M_2 - M_1)\omega^2}{2kT_i} . \tag{10}$$

The enrichment factor expresses the fact that centrifugal separation depends exponentially on the ratio of the difference in ordered rotational kinetic energies of the isotopes and the random thermal energy. It also shows that the separation increases exponentially as the square of the radial distance from the plasma column axis. However, the Gaussian density distribution implies that the majority of the particle flux is concentrated in a region near the plasma axis.

Similarly for the electrons, if the equation of state $p_e = n_e kT_e$ is adopted, then

$$\begin{aligned} n_e(r) &= n_e(0) \exp\left[\frac{e}{kT_e}\left(\phi(r) - \frac{\omega_e B r^2}{2}\right) + \frac{m_e\omega_e^2 r^2}{2kT_e}\right] \\ &\approx n_e(0) \exp\left[\frac{e}{kT_e}\left(\phi(r) - \frac{\omega_e B r^2}{2}\right)\right] \end{aligned} \tag{11}$$

for $m_e/M_i \ll 1$.

The ion momentum equation can also be solved to provide the bulk rotation frequency ω_i of the plasma ions,

$$\omega_i = \Omega_i \left[-\frac{1}{2} \pm \frac{1}{2}\sqrt{1 + \frac{4}{\Omega_i B}\left(\frac{d\phi(r)}{rdr} + \frac{kT_i}{Z_i e}\frac{d(\ln n_i)}{rdr}\right)} \right] \tag{12}$$

where $\Omega_i = Z_i eB/M_i$ is the ion cyclotron frequency. And using the electron momentum equation, we find for the electron rotation frequency,

$$\omega_e = \Omega_e \left[-\frac{1}{2} \pm \frac{1}{2}\sqrt{1 + \frac{4}{\Omega_e B}\left(\frac{d\phi(r)}{rdr} + \frac{kT_e}{e}\frac{d(\ln n_e)}{rdr}\right)} \right] \tag{13}$$

where $\Omega_e = eB/m_e$ is the electron cyclotron frequency.

The ambipolar potential term $\phi(r)$ in Eqn. (13) results from radial losses of the more mobile electrons and can be approximated by $Z_i e\phi \approx kT_e$. Then the terms on the right are approximately given by,

$$\frac{4}{\Omega_i B}\frac{d\phi(r)}{rdr} \approx \frac{4}{\Omega_i B}\frac{kT_e}{Z_i e a^2} \approx \frac{2m_e}{m_i}\left(\frac{v_{eth}}{\Omega_i a}\right)^2 \approx 2\left(\frac{\rho_i}{a}\right)^2 \tag{14}$$

and

$$\frac{4}{\Omega_i B}\frac{kT_i}{Z_i e}\frac{d(\ln n_i)}{rdr} \approx \frac{4}{\Omega_i B}\frac{kT_i}{Z_i e a^2} \approx 2\left(\frac{v_{ith}}{\Omega_i a}\right)^2 \approx 2\left(\frac{\rho_i}{a}\right)^2 \tag{15}$$

where $a^{-1} = d\ln n(r)/dr$ is the radial density scale length, v_{th} is the thermal velocity, and ρ is the cyclotron radius for the denoted species. Both ratios are small ($2(\rho_i/a)^2 = \epsilon \ll 1$) and the rotation frequencies are given by

$$\omega = \Omega\left[-\frac{1}{2} \pm \frac{1}{2}(1+\epsilon)\right] \tag{16}$$

it is easy to show that the lower frequency root (+) is in fact $\omega \approx E/aB$ *i.e.* the two ion species move at the $\vec{E} \times \vec{B}$ drift velocity. In the high frequency equilibrium (–), the ions rotate opposite to their cyclotron motion, at nearly the cyclotron frequency ($\omega \approx -\Omega_i(1+\epsilon)$), with small perturbations due to the electric field and pressure gradient terms. The fluid rotation frequency scales linearly with the magnetic field and provides a straight forward means of increasing the rotation frequency.

The ambipolar potential can be explicitly found by making the usual assumption that the plasma is quasi-neutral,

$$n_e(r) = Z_i n_i(r)\,, \tag{17}$$

and Eqns. (6)and (12) then yield a parabolic potential for all r, *viz.* :

$$\phi(r) = \frac{T_i T_e}{2e\,(T_i + T_e Z_i)} \left\{ \frac{M_i}{T_i} \left[\Omega_i \omega_i + \omega_i^2 \right] + \frac{m_e}{T_e} \Omega_e \omega_e \right\} r^2 + \phi(0)\,. \tag{18}$$

The parabolic potential when introduced into Eqns. (6)and ((12)) produces an exponent argument proportional to r^2 indicating a Gaussian density profile. In the derivation above, the electron and ion temperatures were assumed to be spatially uniform in which case the electron and ion pressures are also Gaussian. From the potential, the electric field is immediately seen to vary as the radius so that E/rB is a constant and the plasma column rotates as a rigid body.

Rigid rotor equilibria, using fluid models for non-neutral and neutral plasma columns, have been studied extensively. In non-neutral plasmas confined by uniform axial magnetic fields, it has been shown[21] that a rigid-rotor equilibrium leads to parabolic radial potential profile and a Gaussian radial density profile. A similar result was obtained in neutral plasma columns in thermal equilibrium using a rigorous kinetic analysis based on the Vlasov-Poisson equations.[22] A self-consistent fluid model predicted parabolic radial potential profiles[23] in charge- and current-neutralized ion beams propagating axially into a solenoidal magnetic field. These predictions were confirmed by experiments.[24,25] Experimental studies on neutralized ion thrusters, with no applied magnetic field, showed that the density and potential in the beam have Gaussian and parabolic radial profiles, respectively.

Putting in some typical numbers for a carbon plasma: $T = 2\,eV$, $B = 0.2\,T$ and $r_o = 2\,cm$:

$$\epsilon^2 = \left(V_{th}/\Omega r_o\right)^2 \approx 3 \times 10^{-2} \ll 1 \tag{19}$$

At the other end of the periodic table, a thallium plasma with $T = 2\,eV$, $B = 0.5\,\mathrm{T}$ and $r_o = 2\,cm$ gives:

$$\epsilon^2 = \left(V_{th}/\Omega r_o\right)^2 \approx 8.5 \times 10^{-2} \ll 1 \tag{20}$$

Equations (19) and (20) show that for practical values in the vacuum arc centrifuge, the lower rotation frequency $\omega = \epsilon\Omega$ is about a factor of ten lower than the ion cyclotron frequency. The cyclotron frequency is typically $10^6\,rad/s$, hence the lower, $\vec{E} \times \vec{B}$ frequency is about $10^5\,rad/s$. In all the experiments on vacuum arc centrifuges at Yale,[16,26,27] Australia,[28] Brazil,[29] and Israel[30] between 1980 and 1989, only this lower frequency was observed. The Yale group had theoretically examined the possibility of achieving the higher frequency by appropriate modification of the plasma density profile[17] but no experiments were conducted. As with many dynamical equilibria

that allow multiple solutions, the key to achieving a particular equilibrium is to understand the dynamical pathway which must be followed to arrive at that particular solution. In 1989, the Ibaraki University group demonstrated operation at the higher rotation frequency for the first time.[18] One feature of their experiment was a hollow plasma as opposed to a solid plasma profile in earlier experiments by other groups. SRL has been able to reproduce the Ibaraki result, but in a solid plasma configuration.

Equations (13)–(6) show that for either of the two rotational equilibria, the rotational frequencies of the electrons and ions are slightly different. Equation (13) shows that because of the smallness of the electron mass, the centrifugal term is negligibly small and the electrons execute $\vec{E} \times \vec{B}$ drift with only a small correction due to the electron pressure gradient. However, the ions rotate at a different frequency, either in the same direction as the electrons (lower frequency equilibrium) or counter to the electron rotation (higher frequency equilibrium). In either case there is therefore an azimuthal current J_θ in the plasma. This azimuthal current, crossed with the axial magnetic field, provides a $\vec{J}_\theta \times \vec{B}$ Lorentz force acting radially inwards, which balances the centrifugal and pressure gradient forces that act radially outwards, resulting in radial equilibrium of the rotating column. Finite resistivity due to ion-electron collisions leads to a gradual diffusion of the plasma column across the magnetic field. Returning to Eqns. (12)and (6), it is obvious that the azimuthal velocities of ions of different mass/charge ratio are in general different, unless the pressure gradient terms take a special form. Alternatively, if the two ion species rotate at different azimuthal frequencies, there will be azimuthal drag (collisional momentum exchange) due to ion-ion collisions, which in turn will result in radial diffusion. The ion species will redistribute themselves across the column. A small pedagogical point is worth making here. It is well known[31] that in a single ion species plasma, ion-ion diffusion is not as important as ion-electron diffusion. However, Bonnevier[32] showed that in a two-ion species plasma, inter-species collisional diffusion can proceed at rates in excess of classical ion-electron diffusion. Ion-ion diffusion is therefore an important process in plasma centrifuges. Suppose a quasi-equilibrium is reached wherein the net radial flux due to ion-ion collisions is zero *i.e.* both ion species achieve the same rigid-rotor angular frequency. Such a quasi-equilibrium demands a radial redistribution of the ions.

B.3 Separation Characterization

The feed stream to a separator, in this case a plasma centrifuge, is some combination of isotopes. Using standard separation terminology[33] desired isotope has number density n_p

(= n_2) and will be channeled into the product (or heads) stream. All other isotopes constitute the waste (or tails) stream and have number density n_w (= n_1). The total density at any radius r is $n_t(r) = n_p(r) + n_w(r)$ and the product abundance ratio (Eqn. (8)),

$$R_p(r) = \frac{n_p(r)}{(n_t(r) - n_p(r))} = \frac{f_p(r)}{(1 - f_p(r))}$$

where $f_p = n_p/n_t$ is the molar fraction, or alternatively, the concentration of the product isotope. Since the densities on axis are approximately the natural abundances, before separation $R_n \approx R_p(0) = R_{po} = R(0)$. In the centrifuge, product is collected at a radius approximately corresponding to the desired enrichment, defined for a two isotope system as,

$$\gamma(r) = \frac{f_p(r)/(1 - f_p(r))}{f_w(r)/(1 - f_w(r))} = \frac{f_p(r)/(1 - f_p(r))}{(1 - f_p(r))/f_p(r)} = \left(\frac{f_p(r)}{1 - f_p(r)}\right)^2 .$$

so after a single centrifuge, $R_p = R_{p1} = R(r) = \gamma R(0)$. For n cascaded devices the product abundance is $R_{pn} = \gamma^n R_{po}$. Alternatively, for a desired concentration R_{px} corresponding to an enrichment $\gamma_x = R_{px}/R_{po}$, the required number of separation stages is $n = \ln(R_{px}/R_{po})/\ln\gamma$.

The number density in these expressions can be replaced with the mole number or molar fraction, with equal validity. The latter units are more appropriate for thermodynamic relationships in which the concept of separative work units (SWU) is typically presented. With $f_w = n_w/n_t$ is the molar fraction of the waste isotope(s), $1 = f_p + f_w$ and $R_p = f_p/f_w = f_p/(1 - f_p)$ and $R_{pn} = \gamma^n R_{po}$ as before. Similarly, if the feed flow is Γ_f moles per unit time, then $\Gamma_p = f_p\Gamma_f$ is the product flow and $\Gamma_w = f_w\Gamma_f = (1 - f_p)\Gamma_f$ is the waste component flow.

From Eqn. (8) it is clear that both product and waste exist in the various separation stages. To collect the desired product isotope, plasma beyond some radius r_c is skimmed off. The fraction of material collected as product is η, the "cut". Because of conservation of mass,

$$F_{po} = \eta F_{p1} + (1 - \eta)F'_{p1} \tag{21}$$

and

$$F_{wo} = 1 - F_{po} = \eta F_{w1} + (1 - \eta)F'_{w1} \tag{22}$$

where the primed quantities refer to the new waste stream. In each stream, the new mole fractions add to unity. The new mole fractions add to unity. Figure 2 shows graphically the relationship of these quantities.

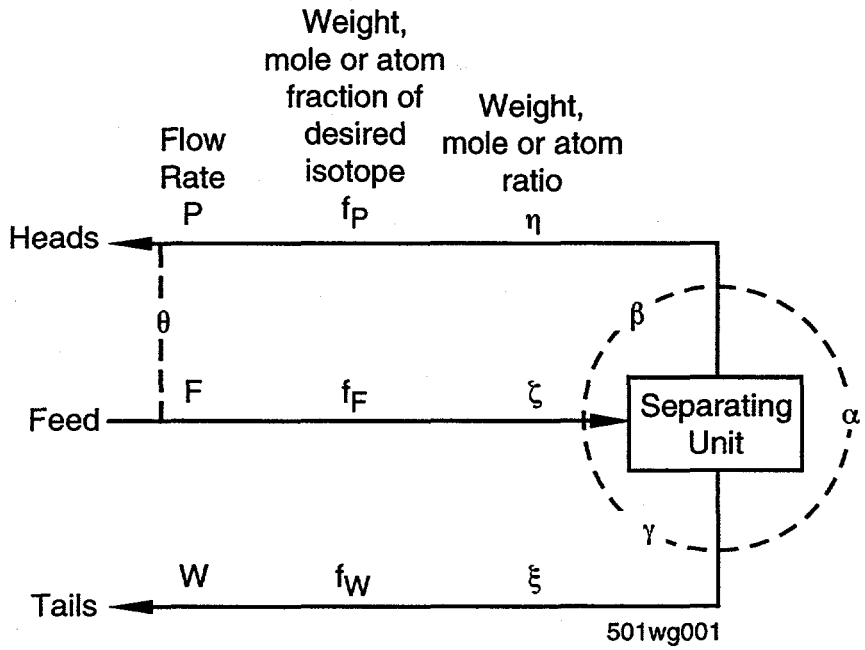

Figure 2: Relationship of flow rates, concentrations, and separation factors (after Ref. 33).

The new product stream $\Gamma_{p1} = \eta\Gamma_{fo}$ has a larger product molar fraction,

$$\begin{aligned} F_{p1} &= \gamma F_{po} \\ &= \gamma(1 - F_{wo}) \end{aligned} \tag{23}$$

and a smaller waste fraction,

$$\begin{aligned} F_{w1} &= 1 - F_{p1} \\ &= 1 - \gamma F_{po} \\ &= 1 - \gamma(1 - F_{wo})\,. \end{aligned} \tag{24}$$

The new waste stream $\Gamma_{w1} = (1 - \eta)\Gamma_{fo}$ has a larger waste molar fraction,

$$\begin{aligned} F'_{w1} &= \frac{F_{wo} - \eta F_{w1}}{1 - \eta} \\ &= \frac{F_{wo}(1 - \gamma\eta + \eta(\gamma - 1)}{1 - \eta}\,, \end{aligned} \tag{25}$$

and a smaller product fraction,

$$F'_{p1} = \frac{F_{po} - \eta F_{p1}}{1-\eta} = \frac{F_{po}(1-\eta\gamma)}{1-\eta} . \tag{26}$$

The performance of both plasma and gaseous centrifuges is characterized by their separative work. The separative work concept is quite general and can be used to characterize an individual separation device as well as a large facility comprised of successive separation steps without regard to the process details. A separation process seeks to decrease the entropy S of the feed stream and the usefulmess of a separation process is gauged by the entropy decrease it produces. The original mixture of isotopes has a higher degree of disorder than the more ordered separate mixtures of individual isotopes. Along with the entropy decrease, an amount of work $\Delta W = T\Delta S$ is expended for an isothermal process which characterizes the centrifuge. Although the SWU has a name that suggests a relation with the thermodynamic work, it is defined differently and has units of mass flow.

The concept of entropy of separation which is separated into a product stream of abundance $\gamma\zeta$ and a waste stream of abundance γ/ζ. Separative work of a device or process is the work required per mole to change the abundances from the initial abundance to the realized or desired value and is given by[34]

$$\Delta U = \frac{\gamma - 1}{\gamma + 1} \ln\zeta . \tag{27}$$

Dirac[35] showed that independent of the method of operation, the maximum output in separative work units of a centrifuge per unit time is,

$$\delta U_{max} = \pi \rho r Z \left(\frac{\Delta M_i v_\theta^2}{2RT} \right)^2 , \tag{28}$$

where r is the radius, ρ is the mass density, z is the centrifuge length, and R is the universal gas constant. The ratio of the theoretical maxima for the plasma and gas centrifuges is,

$$\frac{\delta U_p}{\delta U_g} = \frac{\rho_p r_p Z_p v_{\theta p}^4 T_g^2}{\rho_g r_g Z_g v_{\theta g}^4 T_p^2} . \tag{29}$$

Typical values[36] for uranium in a supercritical gas centrifuge are shown in Table III. The aspect ratio (length/diameter) is large ≈ 20 with length of $\approx 3.5\,m$ and diameter $\approx 0.18\,m$. Operation for these centrifuges is above the second critical flexure rotational frequency $\approx 500\,Hz$. Rather than pure uranium, uranium hexafluoride UF_6 is found to be more convenient which has a vapor

pressure at room temperature ($27°C$) of $128\,Torr$. In American gas centrifuge machines, the uranium output has been reported[34] to be $\approx 100\,kgSW/yr$. Using values in Table III for the present SRL device and the gas centrifuge, the maximum separative work ratio for the plasma and gas centrifuges (Eqn. (29)) is $\approx 1.2 \times 10^5$. The largest difference between the two devices is the rotational velocity which enters as v_θ^4. While neither centrifuge would realize its maximum theoretical value, the plasma centrifuge has a clear advantage. Some improvements in the plasma centrifuge are possible for a production device, however they would be modest.

Table III
Separative Work Comparison for Various Centrifuges

	Gas	VAC Plasma (Present)	VAC Plasma (Production)
$r_c\,(m)$	0.09	0.025	0.05
$n_U\,(m^{-3})$	4.5×10^{24}	1×10^{20}	2×10^{20}
$T\,(°K)$	300	2.3×10^4	7×10^4
$v_\theta\,(m/s)$	3×10^2	3.75×10^4	5×10^4
$Z\,(m)$	5	1	2

B.4 SRL Centrifuge Description

The major accomplishments of the Phase II program are presented in the this section. Construction of the plasma centrifuge and the upgrading to high repetition rate progressed as outlined in the Phase II proposal. The important aspects of the plasma rotation and collection were verified.

A schematic of the prototype centrifuge constructed in Phase II is shown in Fig. 1 and pictured in Fig. 3 and Fig. 4. The design and construction effort was led by Dr. M. Krishnan and Dr. R. Prasad who helped pioneer the plasma centrifuge concept. The support base below the magnets measures $2.25\,m$ long and $0.9\,m$ wide, and the magnet coils have an outer diameter of about $0.8\,m$. The support base contains a mechanical vacuum pump which exhausts the turbomolecular pumps, and the Nd:YAG laser which initiates the cathode discharge and the laser beam optics for transport and focusing.

The principal subsystems are the vacuum-arc source and its power supply, the magnetic field coil and its power supply, the isotope collection mechanism, the vacuum system, and the diagnostic and data acquisition system. Each subsystem was fabricated using readily available

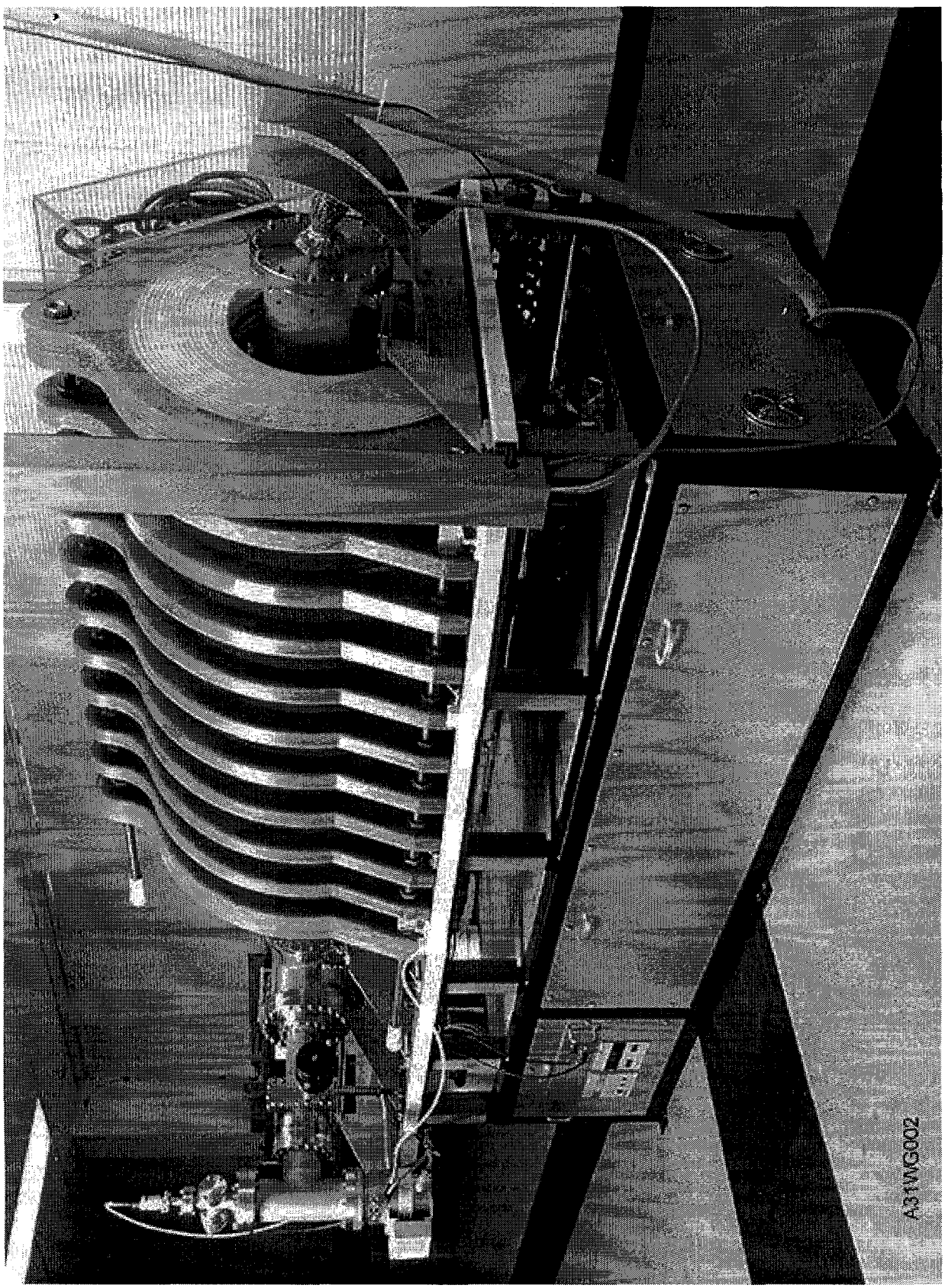

Figure 3: Vacuum-arc centrifuge device viewed from the cathode end.

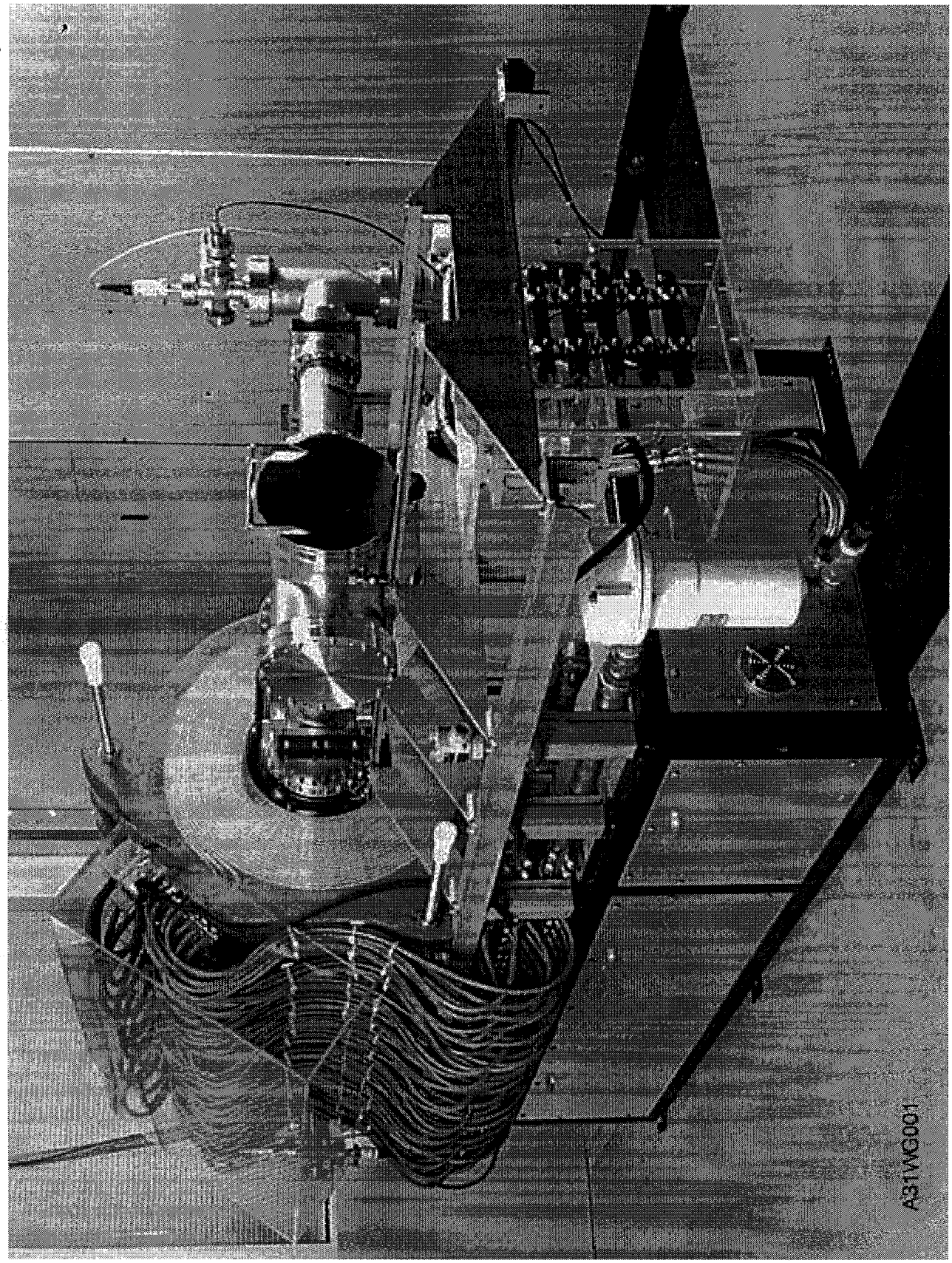

Figure 4: Vacuum-arc centrifuge device viewed from the collector end.

components which facilitates the commercialization of the plasma centrifuge.

The source is a vacuum-arc which produces a fully ionized plasma. The source is currently operated with a voltage pulse of duration $\approx 10\,ms$ at up to a $5\,pps$ repetition rate. A pulse forming network (Fig. 5) produces the voltage pulse. In initial experiments, the PFN was powered by a capacitor bank and was limited to $\approx 10^{-3}\,pps$. The source and its associated power supplies have recently been upgraded by SRL to permit high repetition rate ($5\,pps$) operation through the addition of water cooling to the cathode and to the PFN components. At present, the PFN is charged from a DC power supply with maximum ratings of $200\,V$ and $200\,A$. As indicated in Fig. 5, the power supply charges the PFN with a short current pulse. At the time of the discharge initiation, the power supply is disconnected from the PFN to avoid it having to drive the very low impedance plasma. The vacuum-arc constitutes the switch that discharges the PFN and is initiated by either a high power laser pulse (Fig. 1) or by a high voltage spark. The laser produces a $1.5\,J$, $8\,ns$ pulse focused on the cathode. The PFN produces the cathode voltage shown in Fig. 6. The initial cathode-anode voltage equals the charge voltage of $\approx -200\,V$, and during the quasi-steady portion of the pulse the cathode voltage decreases to approximately half the initial value for a plasma resistance of $\approx 35\,m\Omega$. A typical cathode current waveform is shown in Fig. 7. For the typical pulse shown in Fig. 7, the time integrated current yields a charge of $\approx 35\,C$. The improved PFN allows much more rapid collection of isotopes. For a $1\,g$ collection of ^{26}Mg, only about 60 minutes is required at $3\,kA$ and $5\,pps$ operation.

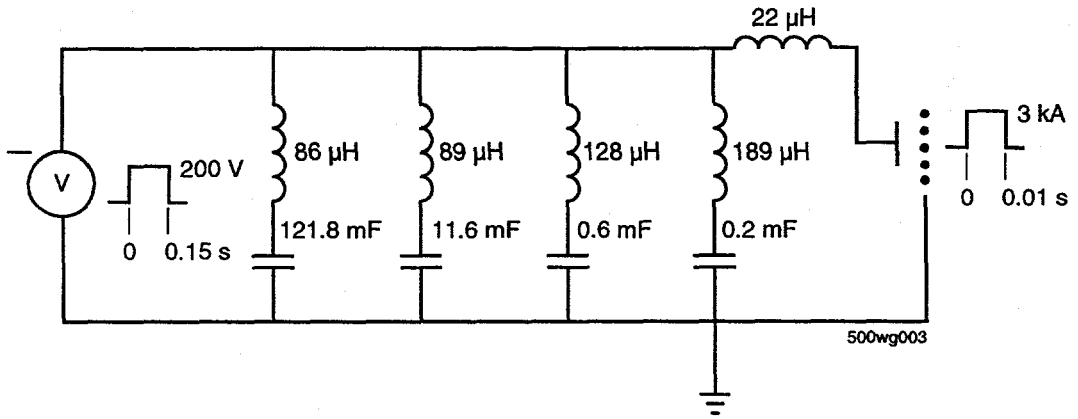

Figure 5: Circuit diagram of the pulse forming network which biased the centrifuge cathode.

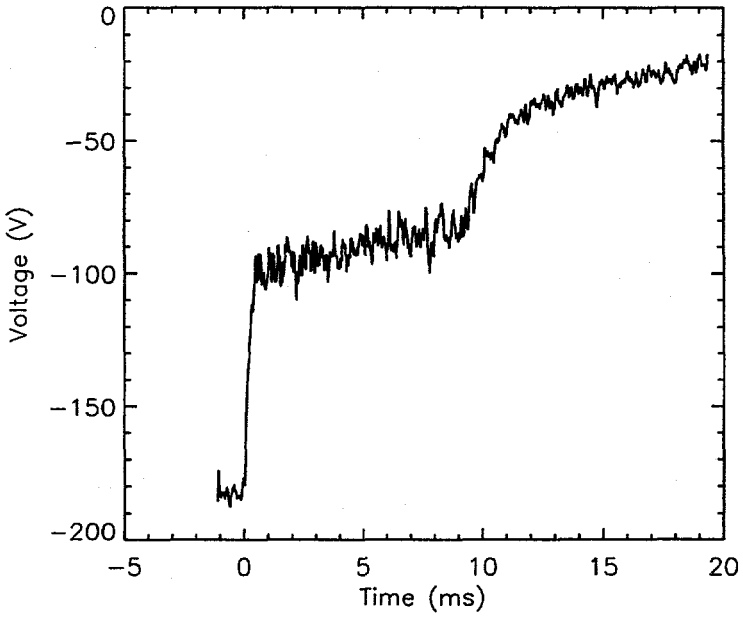

Figure 6: Cathode voltage during discharge in the plasma centrifuge.

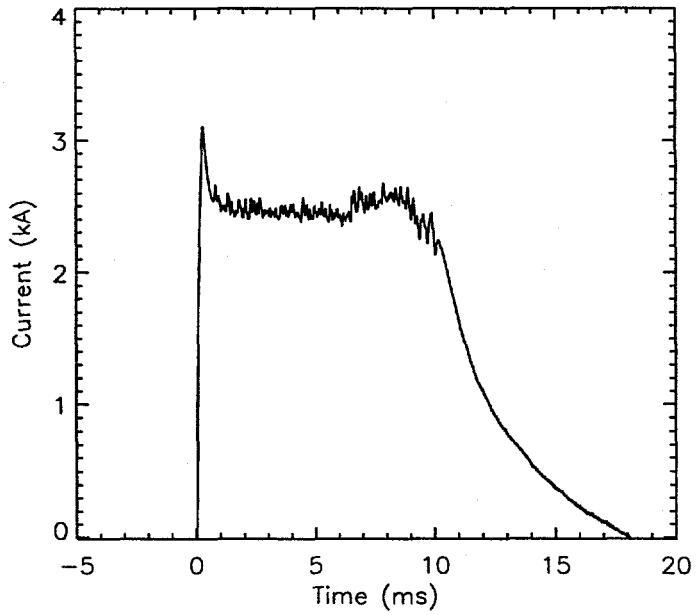

Figure 7: Cathode current during discharge in the plasma centrifuge.

In the present source configuration, the cathode is made of the raw material whose isotopes are to be separated, and an anode, presently a tungsten mesh with about 50% transmission. During Phase II, the cathode materials have been machinable materials, specifically carbon and magnesium.

Figure 8 shows a used magnesium cathode from the centrifuge developed in Phase II. The solid cylindrical cathode allowed convenient collection of heavier isotopes from the feed stream. The isotopic abundances are ^{24}Mg 79%, ^{25}Mg 10%, and ^{26}Mg 11%. The cathode has a maximum diameter of 2.5 cm. The small cylindrical end provides a path for electrical and thermal conduction and was attached to a water cooled stalk leading to a ceramic vacuum feedthrough.

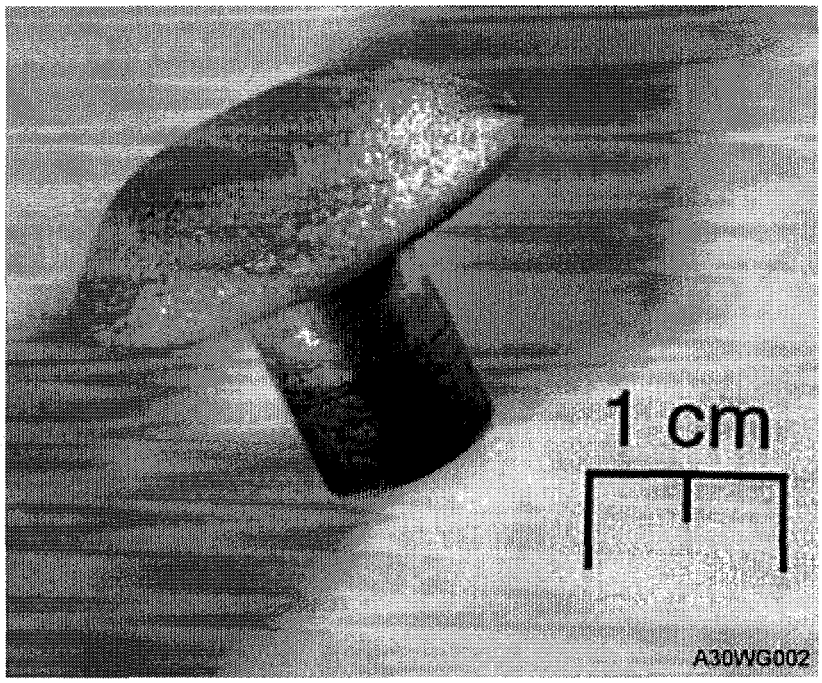

Figure 8: Photograph of a used magnesium cathode. The dark spot on the right edge is the laser focus point.

A magnetic field is required to produce the plasma confinement and rotation. The set of magnetic field coils shown schematically in Fig. 1 is shown in more detail in Fig. 9. The actual coils have a high aspect ratio cross section allowing easy access to the vacuum vessel ports for diagnostics and maintenance. As points of reference, diagnostic ports were located at $z = 40\,cm$ and $z = 90\,cm$. A chilled water supply cools the coils (Fig. 4) allowing continuous coil operation. Each coil contains four pancakes, connected in series, of 17 turns each. In turn, all the coils are connected in series to form a solenoid. The total coil resistance was 0.5 Ω. Shunts were used to measure the coil current and their voltages included in the data set on each recorded pulse.

The coils produce an approximately uniform axial magnetic field along the length of the centrifuge. Figures 10, 11, and 12 show the magnetic field characteristics. Magnetic surfaces are

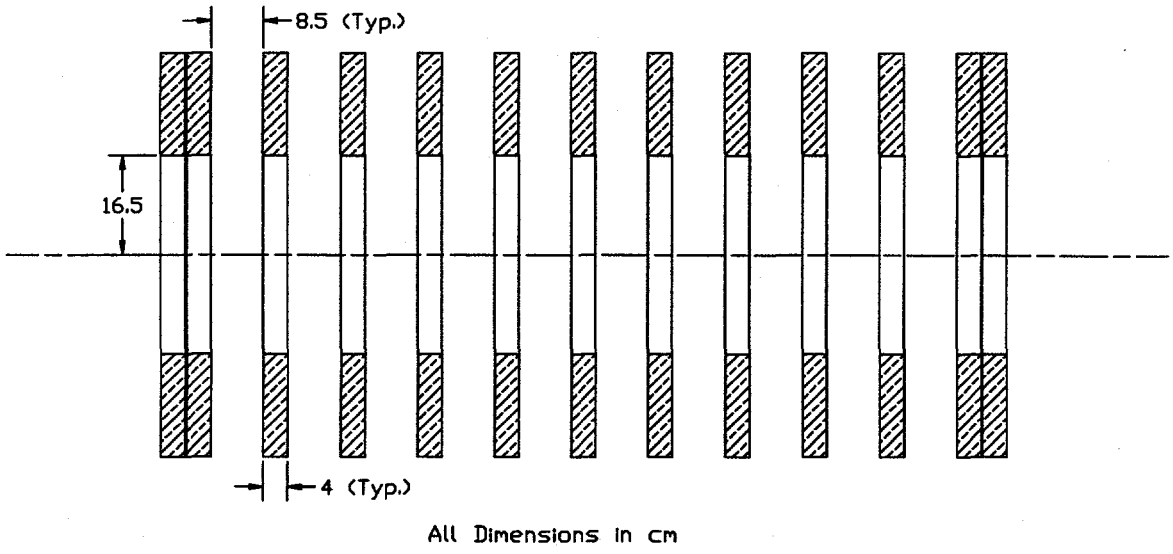

Figure 9: Solenoidal magnetic coil diagram.

defined for values of constant flux ψ where

$$\psi(r) = 2\pi \int_0^r B_z(\rho)\rho \, d\rho \,, \tag{30}$$

where ρ is the radius.of these surfaces are shown in Fig. 10 as a function of axial position z. Coil location and relative current direction are indicated near the top of each figure. The cathode is located at $z = 0$ and the mesh anode is at $z = 15\,cm$. The three surfaces correspond to cathode magnetic flux values at radii of $r_1 = 1\,cm\,(\psi_1)$, $r_2 = 2\,cm\,(\psi_2)$, and $r_3 = 3\,cm\,(\psi_3)$. The normalized flux value for the inner surface is $\psi_1 = 3.68 \times 10^{-8}\,Wb/A$. The axial magnetic field component, B_z, on each flux tube is shown in Fig. 11. Because of the radial uniformity of the axial field, the curves overlay each other. The magnitude of the axial component depends somewhat on the isotope being separated but is $0.1 - 0.2\,T$. Figure 12 shows the axial profile along each flux surface of the radial magnetic field component, B_r.

Near the cathode, the magnetic field is purposely manipulated to produce a large radial component in the anode-cathode gap. The azimuthal force $\vec{F}_\theta$ on the plasma column which spins the plasma column up is given by,

$$\begin{aligned} \vec{F}_\theta &= (\vec{J} \times \vec{B})_\theta \\ &= J_r B_z + J_z B_r \,. \end{aligned} \tag{31}$$

Early plasma centrifuge experiments had uniform axial fields and relied on the first term to generate column rotation. While the axial magnetic field was large, the radial current was a result of radial

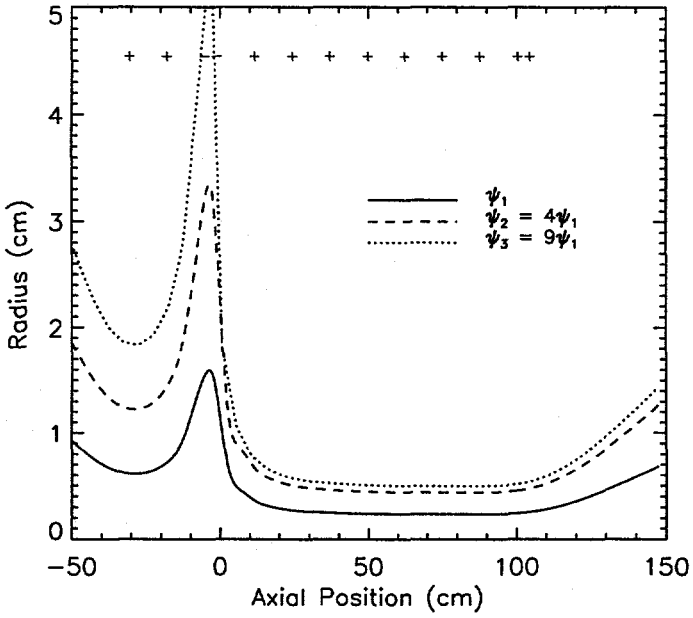

Figure 10: Radius of magnetic flux surfaces as a function of axial position z. Coil locations and relative current direction are indicated at the top of the figure.

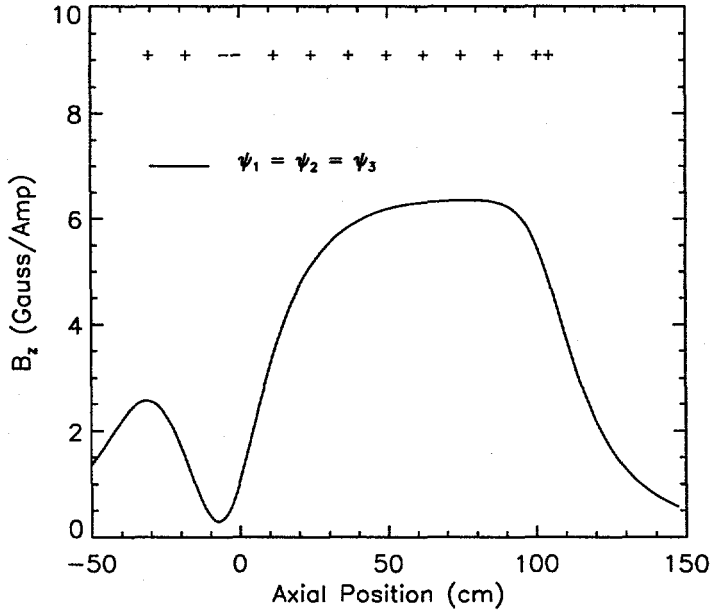

Figure 11: Axial magnetic field on surfaces of constant magnetic flux. Coil locations and relative current direction are indicated at the top of the figure.

ion losses and was small. SRL was successful in reaching the high rotation equilibrium by creating

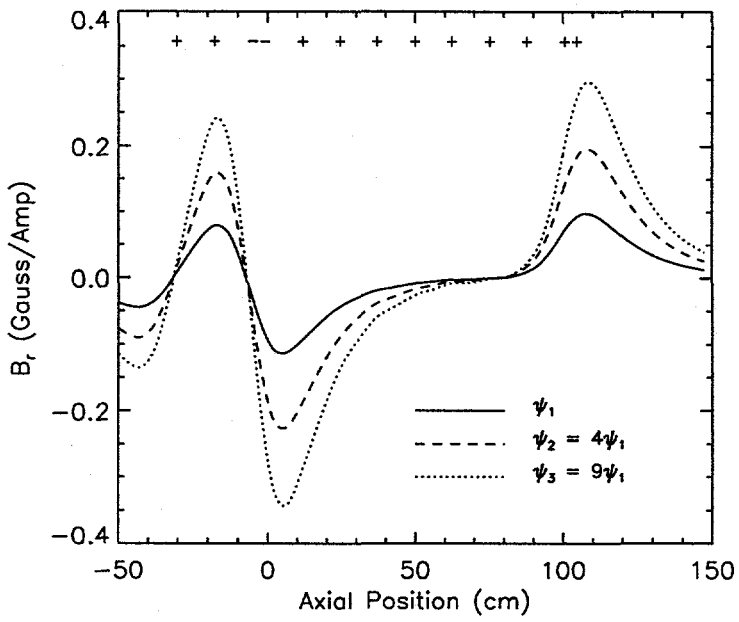

Figure 12: Radial magnetic field on surfaces of constant magnetic flux. Coil locations and relative current direction are indicated at the top of the figure.

a significant radial magnetic field component cathode-anode region where a significant axial current was present and allowing the second term to dominate.

The vacuum vessel is shown in Fig. 13. Standard vacuum components were utilized to fabricate the vessel. Radial diagnostic and maintenance access was provided by the rectangular ports distributed along the vessel length and circumference. Vacuum conditions are maintained using two turbomolecular pumps which maintained a base pressure below $1 \times 10^{-7}\, Torr$ or a neutral density of $n_o \lesssim 3.5 \times 10^9\, cm^{-3}$. During low repetition rate operation, the pressure increased a factor of 2-5, but did not affect the operation of the source or the centrifuge. At the highest repetition rate, pressure increase of a factor of 10 were observed. If for some reason vacuum must be broken, operating conditions were obtained within several hours after starting pump down.

A suite of diagnostics was assembled for the detailed plasma measurements appropriate for the Phase II program. External to the vacuum chamber, the cathode voltage and current are monitored to determine discharge reproducibility and power input into the plasma. Diagnostics to characterize the plasma included Langmuir probes and a $0.5\, m$ scanning monochromator/spectrometer. Not all of these diagnostics would be used on the commercial version of the plasma centrifuge. At high pulse repetition rates, invasive diagnostics such as Langmuir probes would melt under the

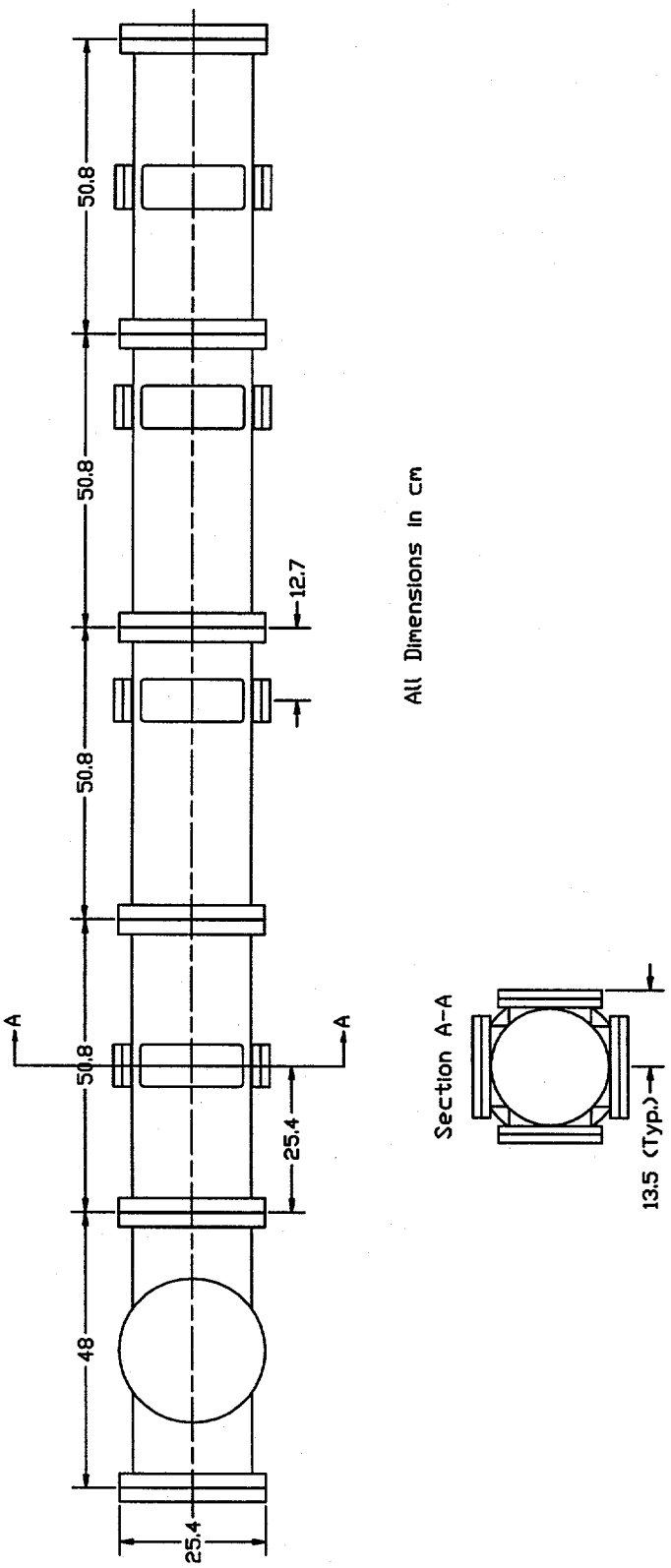

Figure 13: Vacuum vessel diagram.

plasma heat load. Data from the diagnostic suite was collected and digitized using slow ($\approx 10\,kHz$) and fast ($\approx 100\,MHz$) digitizers. Most data was sent to the slow digitizers. However, in order to monitor the rotation frequency, Langmuir probe data was sent to the fast digitizer. Data was then read into a VAX 3100 workstation where it was stored and analyzed. For instance, the Langmuir probe data was Fourier analyzed to determine the frequency spectrum and thus the plasma rotation frequency. For single shot operation, all signals can be stored and analyzed for each shot. For high rep-rate operation, only an occasional discharge was monitored and stored. Currently about 6500 discharges are archived.

B.4 Plasma Characterization

To successfully design future centrifuges, the physics model presented in Section A.2 needs to be compared to the results. Comparisons between the model and the data produce refinements to the model which in turn impact the device design. Many of the features of previous research have been observed on the SRL plasma centrifuge. A noteworthy exception was the rotation frequency which was a factor of 10 higher than previous results from experiments in this country. The following section presents the details of the plasma characterization. Results presented below are representative of operation with a magnesium cathode and for ^{25}Mg and ^{26}Mg separation.

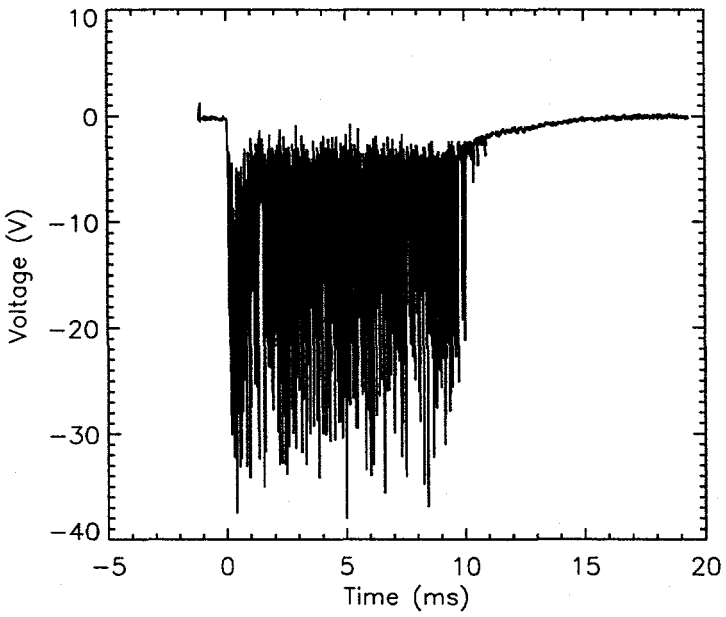

Figure 14: Floating potential during a discharge at $r = 2.5\,cm$.

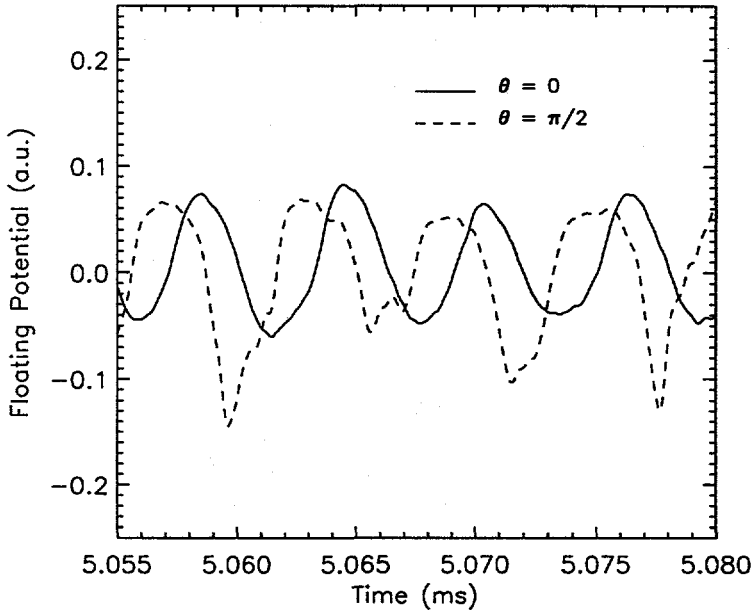

Figure 15: Langmuir probe measurements at $r = 3.0\,cm$ and two azimuthal locations separated by $\Delta\theta = \pi/2$.

A typical electrostatic probe measurement of the plasma fluctuations is shown in Fig. 14. Previous research[26] has shown that the frequency of these electrostatic probe fluctuations are a measure of the rotation of the plasma column and that Doppler shift measurements of the rotation frequency agree with the rotation velocity inferred from probe measurments. Since the two measurements give equivalent information, the probe measurements were preferable since the equipment is simple and well characterized and easy to use in multiple locations. In order to use probe measurements of the rotation frequency with confidence, the plasma fluctuations first needed to be identified. The centrifuge magnetic field topology is approximately that of a simple solenoid and consequently is unstable[37] to magnetohydrodynamic (MHD) modes. Relative to the plasma, the MHD instabilities perturb the plasma boundary and hava a phase velocity $v_\phi = 0$. The plasma boundary distortions therefore move with the plasma and would be a measure of the bulk plasma motion. In the laboratory frame, the moving plasma boundary is a wave with an amplitude that varies as $\exp(\vec{k} \cdot \vec{r} - \omega t) = \exp(k_\theta \theta + k_z z - \omega t)$ where $m = k_\theta r$ is the azimuthal mode number. MHD instabilities can have many different k_z and k_θ values but the smaller values are energetically favored. A typical mode seen in magnetic mirror and pinch confinement geometries is the 'flute' mode[38] which has the characteristics of $k_z = 0$ and some low value of m. The name for this MHD mode is derived from its similarity to a fluted architectural column.

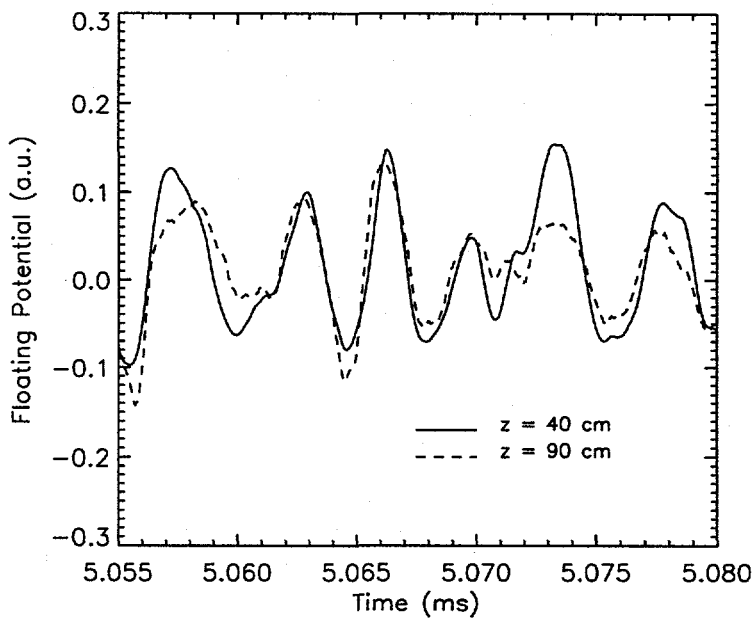

Figure 16: Langmuir probe measurements at $r = 3.0\,cm$ and two axial locations separated by $\Delta z = 50\,cm$.

Measurements were made in the centrifuge at several azimuthal and axial locations to determine the fluctuation wavenumbers in the azimuthal (k_θ) and axial (k_z) directions. The results of the probe measurements are shown in Fig. 15 and Fig. 16 for $t \approx 5\,ms$ and $r = 3.0\,cm$. Fluctuations in the azimuthal direction measured at two azimuthal locations separated by $\Delta\theta = \pi/2$ indicate a phase difference of $\Delta\phi = \pi/2$ which gives an azimuthal mode $m = 1$. In the axial direction, the fluctuations were measured a locations separated by $\Delta z = 50\,cm$, half the plasma length, and there is no observable phase difference. These results imply a MHD flute mode with $k_z = 0$ and $m = 1$ which is consistent with the earlier studies[26].

To obtain the rotation frequency from Fig. 14, the Langmuir probe fluctuation data was Fourier analyzed giving the bulk plasma rotation frequency (Fig. 17). Data taken along a radius are shown in Fig. 18. The error bars indicate the full frequency width at half maximum of the FFT peak (Fig. 17). Although the rotation frequency is not the highest observed, within the uncertainty of these measurements, the plasma column rotates as a rigid body in agreement with the analytic model. Figure 18 also shows that radial probe insertion or other small perturbation does not change the rotational characteristics. These data show that changes in the centrifuge operation are not expected when an isotope collection device which would necessarily have radial components, is inserted.

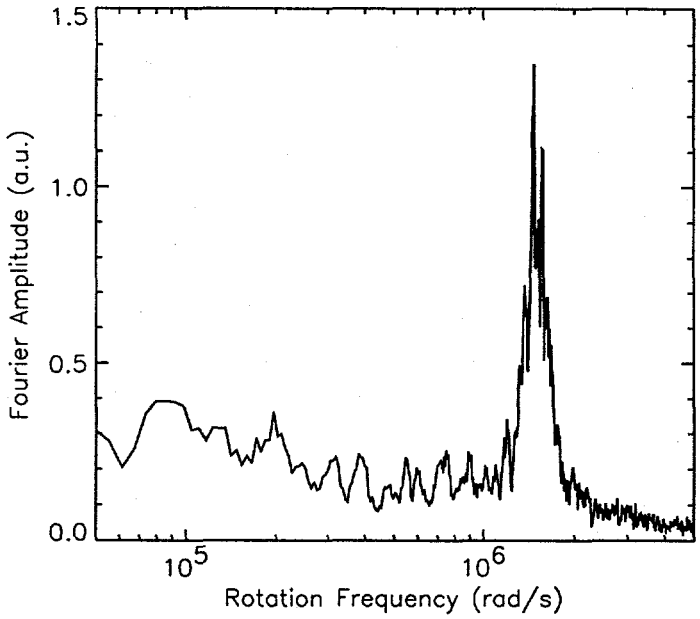

Figure 17: Fourier transform of the floating potential.

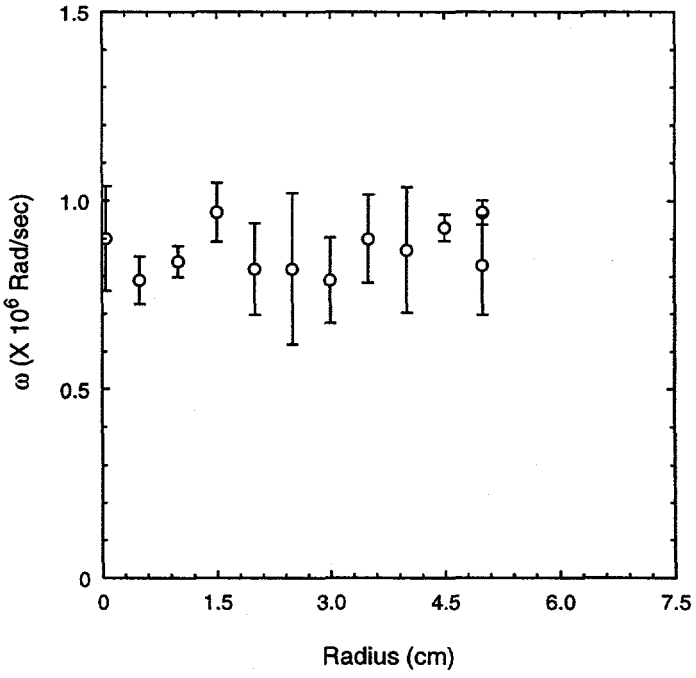

Figure 18: Radial profile of plasma rotation frequency.

The rotation frequency is consistent with the higher rotation equilibrium, $\omega_\theta = \Omega_i$. The axial magnetic field during these measurements was $2.5\,kG$ and consequently the magnesium-ion cyclotron frequency was $\omega_\theta = 1.5 \times 10^6\,rad/s$. Ions rotating at this frequency located at $r = 3\,cm$

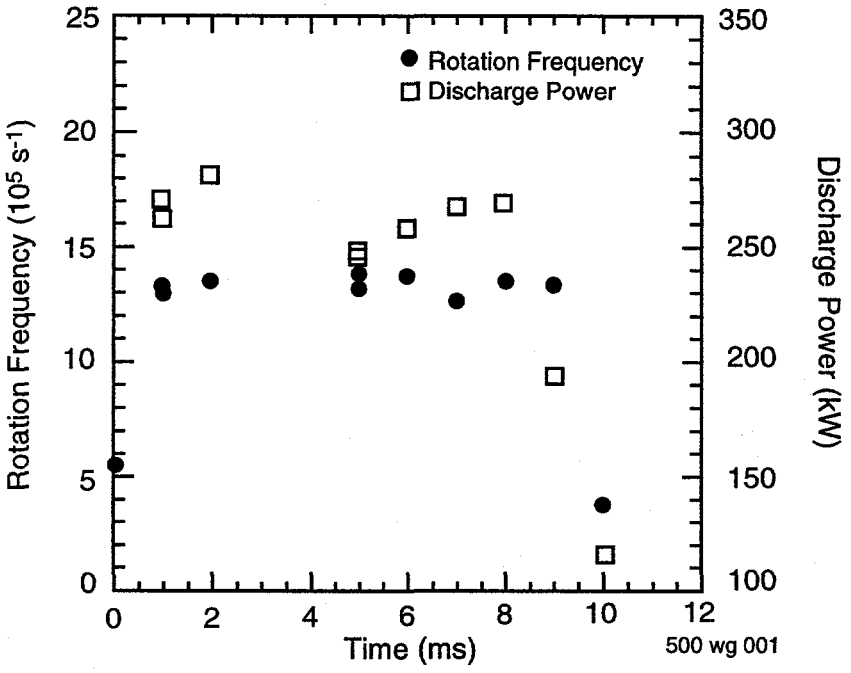

Figure 19: Azimuthal rotation frequency at $r = 3.0\,cm$ and discharge power during the discharge.

have a rotational kinetic energy $E_{\theta i} = 500\,eV$.

The rotation frequency was determined at time intervals throughout the voltage pulse (Fig. 6) and are shown in Fig. 19. The rotation frequency rises immediately upon application of voltage to the cathode and remains quasi-steady until the cathode voltage falls. Since the radial distribution of isotope abundances is velocity dependent, having constant rotation velocity ensures that the relative abundances will remain the same in successive discharges. As a result, high duty-factor, high repetition-rate operation is possible.

Plasma density information was obtained from Langmuir probe ion-saturation current measurements. The temporal density behavior is shown in Fig. 20. The quasi-steady state density $n \approx 10^{14}\,cm^{-3}$ which agrees with density values inferred from the observed cathode erosion rate.

The plasma was also studied spectroscopically. For the magnesium plasma, the emission lines observed at $z = 40\,cm$ are shown in Fig. 21. Only lines identifiable as neutral (ionization potential $\phi_I = 7.66\,eV$) and singly ionized ($\phi_{II} = 15.03\,eV$) magnesium were observed. Lines from doubly ionized ($\phi_{III} = 80.12\,eV$) magnesium in the range of the spectrometer, $491.6\,nm$, $584.0\,nm$, and $625.6\,nm$ were not observed. None of the observed lines corresponded to elements other than the cathode material indicating that the plasma does not become contaminated with other

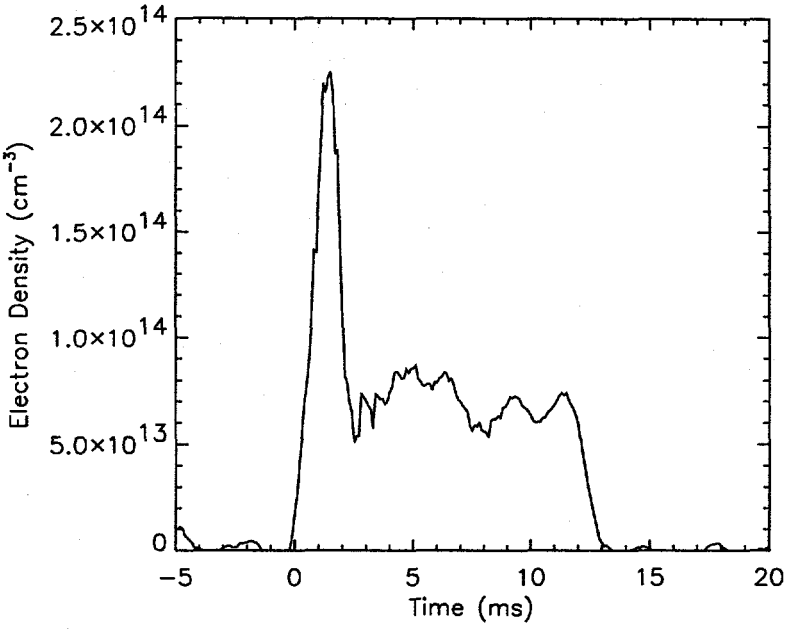

Figure 20: Plasma density at $z = 90\,cm$.

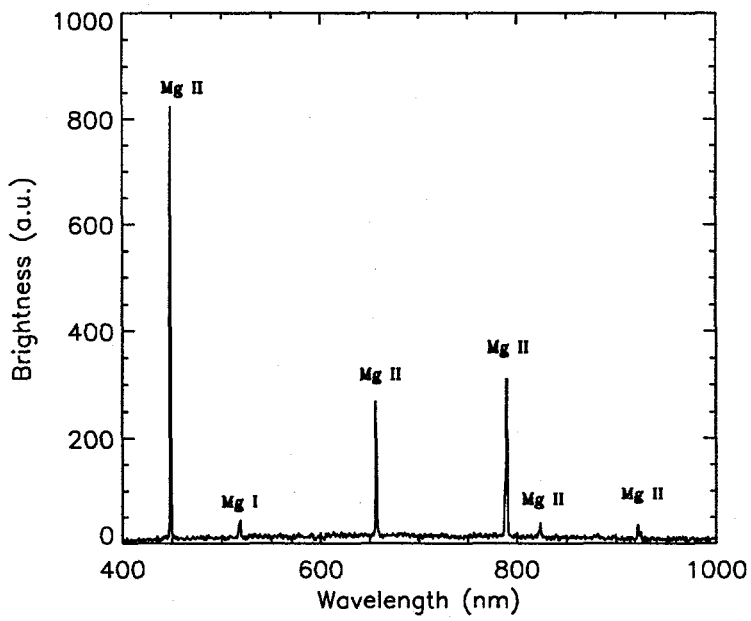

Figure 21: Spectrograph of the magnesium plasma at $z = 40\,cm$.

material. The temporal radiation behavior is shown in Fig. 22 along with the discharge current.

The electron temperature was determined from two measurements, one of which was spectroscopic. Intensity data for line ratios of successive ionization states provided the temperature

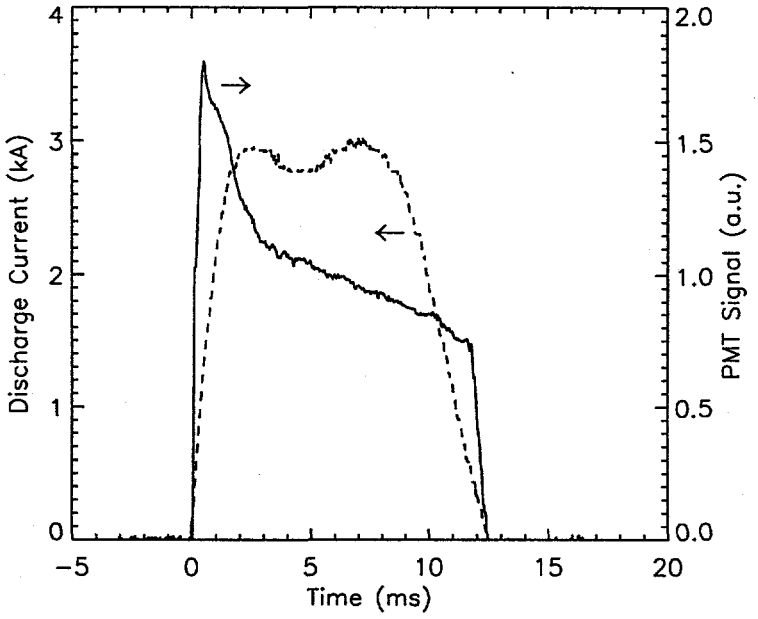

Figure 22: Temporal behavior of the plasma radiation and the discharge current.

measurement. The prominent magnesium lines are shown in Fig. 13. Two lines 517.8 nm (Mg I) and 448.1 nm (Mg II) were monitored and their intensity ratio compared to an analytic expression[39] which is shown in Fig. 23. These particular lines were selected because of their close proximity which minimizes effects of spectrometer sensitivity variations with wavelength. An electron temperature of $\approx 1\,eV$ was determined at $\approx 5\,ms$ by this technique.

Verification of the spectroscopic temperature was made from the plasma resistivity. When the plasma in the anode-cathode gap is assumed to be fully ionized, electron-ion collisions dominate and the resistivity can be described by Spitzer[40],

$$\eta = \frac{\pi e^2 m_e^{1/2}}{(4\pi\epsilon_o)^2 (kT_e)^{3/2}} \ln\Lambda \tag{32}$$

where $\ln\Lambda$ is the Coulomb logarithm and incorporates a finite length cutoff to the Coulomb interaction. In turn,

$$\Lambda = \frac{12\pi}{e} \left(\frac{\epsilon_o k T_e}{n_e e^2} \right) . \tag{33}$$

For the important case of Coulomb collisions, the resistivity is not a function of the plasma density. Using the plasma dimensions and the length of the anode-cathode gap and the cathode voltage and current, the electron temperature was determined to be $1 - 2\,eV$ during the quasi-steady state portion of the discharge.

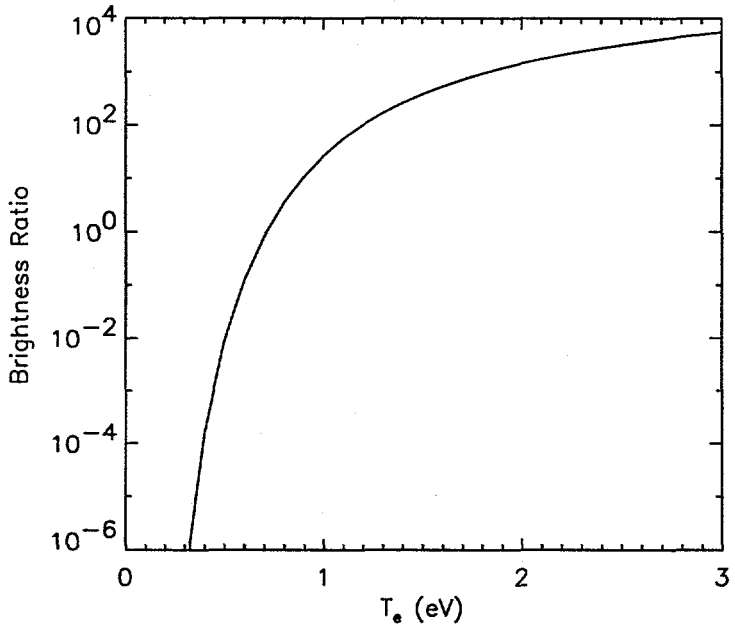

Figure 23: Theoretical brightness ratio for $517.8\,nm$ (Mg I) and $448.1\,nm$ (Mg II) as a function of electron temperature.

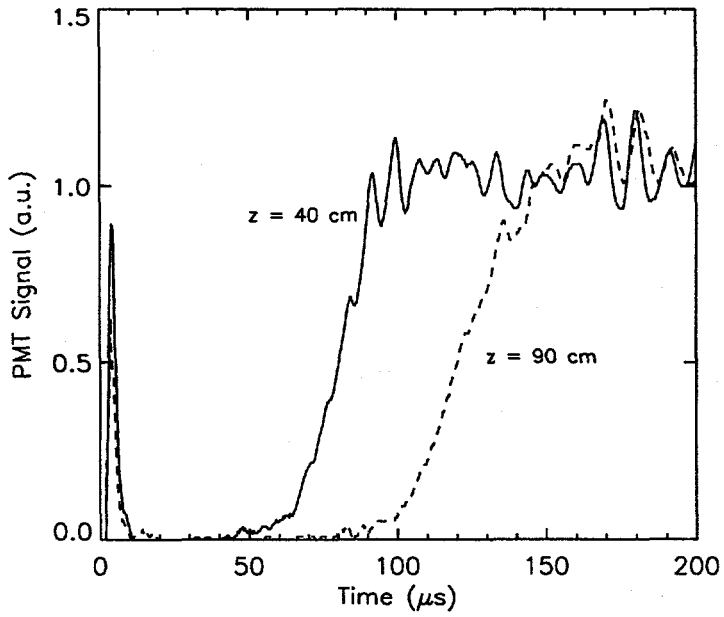

Figure 24: Photomultiplier signals at $z = 40\,cm$ and $z = 90\,cm$.

Figure 24 shows the plasma radiation detected with photodiodes for two axial locations separated by $50\,cm$. The delay time for comparable intensity levels yields is $\approx 38\,\mu s$ implying an axial expansion speed of $1.3 \times 10^6\,cm/s$. The plasma is expected to expand along the axial

magnetic field at the ion sound speed, $v_{si} = \sqrt{2kT_e/m_i}$. The observed expansion speed implies an initial $T_e \approx 30\,eV$ which is much larger than the value determined later during the discharge. The higher value is consistent with a breakdown model where initially the plasma density is small, collisions infrequent, and T_e large. The early spike in radiation (Fig. 22) is also consistent with this scenario. Then the density increases and the electron collision frequency increases and their equilibrium temperature decreases.

The crucial test of the plasma centrifuge was verifying its ability to separate isotopes of the same element. A separation using magnesium was performed at low repetition rate and high rotation frequency ($\omega = 1.6 \times 10^6\,rad/s$). A nonconducting (plastic) 'finger' was inserted to different radial locations and coated with magnesium. A secondary ion mass spectrometry (SIMS) analysis showed an enrichment factor consistent with the rotation frequency. Both isotopes ^{25}Mg (Fig. 25) and ^{26}Mg (Fig. 26) exhibited substantial enrichment. The enrichment factor (Eqn. (9)) is $\gamma = \exp(\alpha)$ where α is the separation factor (Eqn. (10)). For a $\Delta M = 2$ is given by

$$\alpha_2 = \left(\frac{M_{24}Mg}{12}\right)\frac{\omega^2}{2kT_i}\,. \tag{34}$$

The separation factor for $\Delta M = 1$ is $\alpha_1 = \alpha_2/2$. For comparison, the enrichment factor $\gamma\prime$ from the Yale experiment[26] with its lower rotation frequency $\omega\prime$ is also plotted. In each figure, the fitted normalized plasma density profile is also shown. The amount of ^{26}Mg collected was less than $1\,mg$.

B.5 Phase II Results

Phase II was demonstrably a success. The tasks proposed in the Phase II statement of work were accomplished.

- Construction of the plasma centrifuge utilized standard techniques for all of the major sub-assemblies.
- Operation of the centrifuge has been demonstrated at a repetition rate of $5\,pps$.
- The plasma density and temperature, and rotation rate were measured with standard plasma diagnostics.
- Operation of the centrifuge produced plasma parameters in agreement with the high rotation frequency equilibrium described by an analytic MHD model.

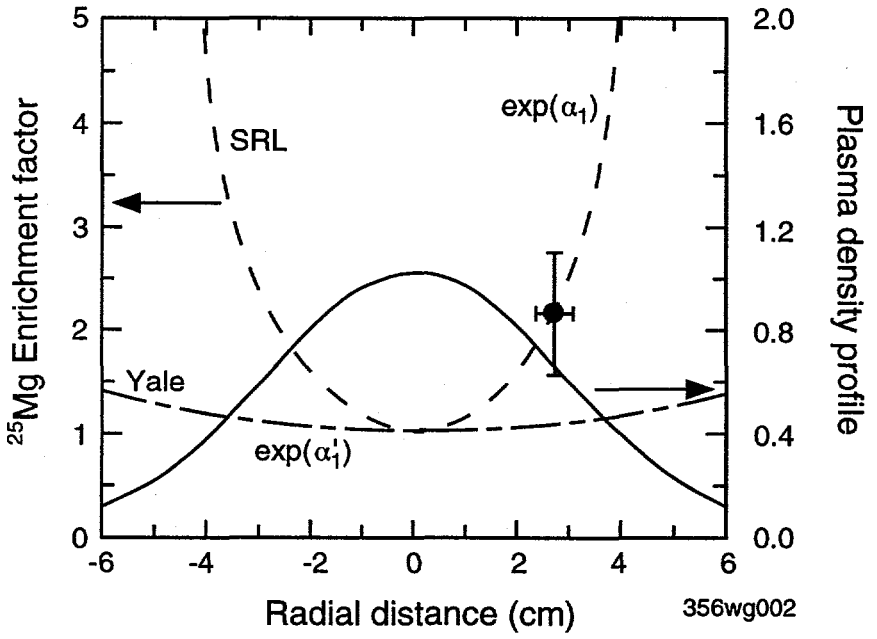

Figure 25: ^{25}Mg enrichment factor and normalized radial density profile.

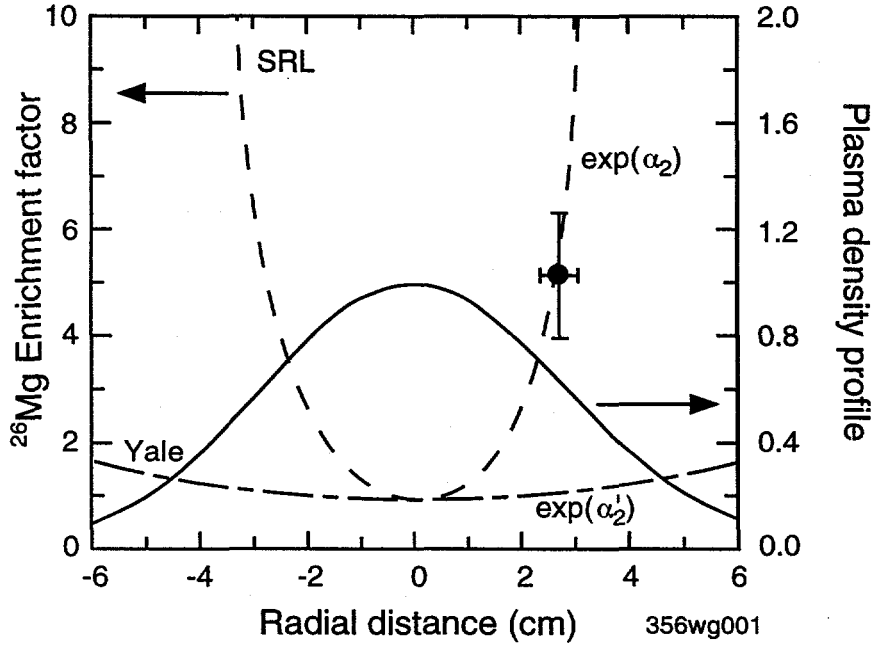

Figure 26: ^{26}Mg enrichment factor and normalized radial density profile.

- A collection in a magnesium plasma was performed which demonstrated isotope enhancement of ^{25}Mg and ^{26}Mg in agreement with the analytic model.

C. PRODUCTION CENTRIFUGE

The next logical step in the development of the SRL plasma centrifuge is to design a production device for moderate scale ($kg/month$) isotope separation. After demonstration of satisfactory operation, this device would be delivered to a DoE facility, perhaps ORNL, for further evaluation. Following satisfactory evaluation, copies or modified versions of the device could be delivered to a customer base which would be identified and established during the prototype phase.

The SRL VAC can process any conducting element or alloy that can be introduced as a solid cathode. Additional elements, for instance gases, can also be processed in the plasma centrifuge upon redesign of the source. Other separation technologies, such as the gas centrifuge or gaseous diffusion require combining elements to produce compounds in the gas phase and may also require separation at elevated temperatures. After separation, the desired isotope must be chemically separated.

Table IV contains the exiting and projected costs for representative stable isotopes. The present costs were obtained from isotope vendors. The projected costs include construction and amortization of a production size unit, the cost of electrical energy, labor costs during separation, and ancillary operating costs. The projected costs assumed:

- PFN voltage $-300\,V$, peak current $4\,kA$, and 25% duty factor
- Discharge power $300\,kW$
- Magnet Power $30\,kW$, vacuum system power $20\,kW$, total electrical power $350\,kW$
- Cathode erosion rate $35\,\mu g/C$ or $108\,g/hr$
- Processing of $1\,kg/10\,hr$ daily
- Energy cost of processed feed $\$0.32/g$
- Enriched product is $1-10\%$ of feed

and lead to an energy cost per separated gram of $\approx \$3-300/g$.

Detailed calculations[26] show that a variety of isotopes useful in nuclear physics and nuclear medicine can be enriched by the plasma centrifuge. For example, with ω = 1.5 x $10^6\,rad/s$ four identical separation stages would enrich ^{203}Tl (an isotope used to produce ^{201}Tl, a 72 hour half-life gamma emitter for cardiography), from its 29.5% natural abundance up to 95%. The fraction of

Table IV
Projected Costs for Selected Stable Isotopes

Isotope (Abundance)	Present Cost ($/g)	SRL VAC Cost ($/g)
^{13}C (1%)	≈ 100	≈ 300
^{26}Mg (11%)	$\approx 2,000$	$\approx 30 - 300$
^{48}Ca (0.18%)	$\approx 50,000$	$\approx 1,600 - 10,000$
^{76}Se (9%)	$\approx 10,000$	$\approx 30 - 300$
^{98}Mo (24%)	–	$\approx 10 - 100$
^{107}Ag, ^{109}Ag (50%)	–	$\approx 5 - 50$
^{111}Cd, ^{113}Cd (12%)	–	$\approx 30 - 300$
^{190}Os (26%)	$\approx 3,000$	$\approx 10 - 100$
^{98}Mo (29%)	$\approx 3,000$	$\approx 10 - 100$

^{203}Tl collected would be 30% of all the ^{203}Tl feed material, or 9% of the total eroded mass.

A practical embodiment of the research device developed at SRL could ionize feed material at a rate sufficient to produce approximately 3 mol/day of enriched thallium. This throughput must be compared with the 0.1 mol/day which is typical of the calutron enrichment process at Oak Ridge National Laboratories[8]. The estimated production cost to enrich ^{203}Tl using the plasma centrifuge is about \$1.50/g. The present market cost of ^{203}Tl is about \$2000/g. Similar estimates lead to a separation cost of about \$40/gram to enrich ^{13}C from 1.1% up to 95%, from a device capable of producing 10 g/day of enriched product. The present market cost of amorphous ^{13}C, enriched to 99%, is about \$250/g.

Several source improvements are required. In order to accommodate gaseous elements, a pulsed plenum could be incorporated. The plenum, actuated with a LC circuit, would introduce a measured amount of gas into the anode-cathode gap. Independent of the cathode design, a significant improvement in the source design would be the elimination of the wire mesh anode. If the source can operate without the mesh, the electrical efficiency (particles/Coulomb) can be improved immediately by about a factor of 2.

The most beneficial alterations to the centrifuge design for increased scale and efficiency are centered at the source. Two modifications would greatly enhance operation. In the discussion above, and for most of the experiments, the cathode was uniform resulting in a plasma density peaked on axis. Because the rotational velocity scales with the distance from the axis, this results

in most of the particles having small velocities. An annular beam would place the bulk of the beam at large radii and take full advantage of the rotational velocity scaling.

The second modification involves the replacement of the mesh anode with an annular anode located outside the plasma but close to its periphery. A thorough analysis of the annular beam includes a determination of possible instabilities. Davidson[22] derives an electrostatic stability theorem for nonrelativistic non-neutral beams which states that a necessary condition for instability is the presence of a positive slope in the radial density distribution. An annular beam clearly satisfies this condition, however, the growth rate for the instabilities may be sufficiently low that in the centrifuge the instability does not grow to an appreciable amplitude. One candidate instability is the diocotron instability. This mode, as well as other instabilities will be investigated as part of the source modification.

The annular anode design can be studied with a well developed computational tool[41] EGUN, which was originally developed for non-neutral particle beams but also includes the option of modeling neutralized beams. The code includes the external, along with the induced azimuthal magnetic fields and the macroscopic electrostatic fields. It does not include the self axial-magnetic field from azimuthal drifts, two-particle effects, or instability effects which would be examined separately.

At present, the magnetic fields are DC and the source electronics runs at up to $5\,pps$ for a duty cycle of 5%. The source itself is a low voltage, low impedance load. For the production device, a new source power supply would be designed to take advantage of these characteristics. This supply would provide power to the source directly from the $408/480\,V$ mains and provide up to a $60\,pps$ pulse repetition rate. For the same pulse length, the duty cycle would increase to about 60%.

D. REFERENCES

[1] *Separated Isotopes: Vital Tools for Science and Medicine*, Ed. by G. Friedlander and H.N. Wagner, Jr., National Academy Press, Washington, D.C., 1982.

[2] R.M. Lambrecht, in *Separated Isotopes: Vital Tools for Science and Medicine*, Ed. by G. Friedlander and H.N. Wagner, Jr., National Academy Press, Washington, D.C., 1982, pp. 185-246.

[3] M.S. Zisman, in *Separated Isotopes: Vital Tools for Science and Medicine*, Ed. by G. Friedlander and H.N. Wagner, Jr., National Academy Press, Washington, D.C., 1982, pp. 81-178.

[4] B.B. McInteer, Sep. Sci. and Tech. **15**, 491 (1980).

[5] *Isotopes in Everyday Life*, Report IAEA/PI/A6E, International Atomic Energy Agency, Vienna, Austria, 1990.

[6] J.D. Gordon, J.J. Thomson, and S.N. Suchard, ANS Meeting, Philadelphia, PA, Dec. 1983.

[7] *Isotopes for Medicine and the Life Sciences*, Ed. by S. James Adelstein and Frederick J. Manning, National Academy Press, Washington, D.C. 1995.

[8] Mark W. Grossman and Thomas A. Shepp, IEEE Trans. Plasma Sci. **19**, 1114 (1991).

[9] J. Slepian, J. Appl. Phys. **26**, 1283 (1955).

[10] B. Bonnevier, Plasma Phys. **13**, 763 (1971).

[11] B.W. James and S.W Simpson, Phys. Lett. **46A**, 347 (1974).

[12] F. Boeschoten and L.J. Demeter, Plasma Phys. **10**, 391 (1968).

[13] B.W. James and S.W Simpson, Plasma Phys. **20**, 289 (1976).

[14] C.J. Walsh, G.F. Brand, and B.W. James, Phys. Lett. **73A**, 109 (1979).

[15] G.F. Brand, B.W. James, and C.J. Walsh, Phys. Fluids **22**, 439 (1978).

[16] M. Krishnan, M. Geva, and J.L. Hirshfield, Phys. Rev. Lett. **46**, 36 (1981).

[17] C. Kim, R. Jensen, and M. Krishnan, J. Appl. Phys. **61**, 4689 (1987).

[18] T. Ikehata, M. Suzuki, T. Tanabe, and H. Mase, Appl. Phys. Lett. **55**, 1289 (1989).

[19] M. Geva, M. Krishnan, and J.L. Hirshfield, J Appl. Phys. **56**, 1398 (1984).

[20] R.R. Prasad and M. Krishnan, J. Appl. Phys. **61**, 4464 (1987).

[21] R.C. Davidson, *Physics of Non-Neutral Plasmas*, Addison-wesley, Redwood City, CA 1990

[22] R.C. Davidson, Phys. Fluids, **19**, 1189 (1976).

[23] S. Robertson, J. Appl. Phys. **59**, 1765 (1986).

[24] S. Robertson, Phys. Rev. Lett. **48**, 149 (1982).

[25] S. Robertson, Phys. Fluids **46**, 1129 (1983).

[26] R.R. Prasad, PhD Thesis, Yale University 1987.

[27] M. Geva, PhD Thesis, Yale University 1982.

[28] P.J. Evans, F.J. Paoloni, J.T. Noorman, and J.V. Whichello, J. Appl. Phys. **66**, 115 (1989).

[29] E. Del Bosco, R.S. Dallaqua, G.O. Ludwig, and J.A. Bittencourt, Appl. Phys. Lett. **50**, 1716 (1987).

[30] M. Geva, C. Cohen, O. Danziger, F. Dotham, L. Friedland, L.A. Levin, S. Maharshak, and J.L. Hirshfield, IEEE Trans. Plasma Sci. **PS-15**, 583 (1987).

[31] C.L. Longmire and M.N. Rosenbluth, Phys. Rev. **103**, 507 (1956).

[32] B. Bonnevier, Ark. Fysik. **33**, 255 (1966).

[33] M. Benedict, T.H. Pigford, and H.W. Levi, *Nuclear Chemical Engineering* McGraw-Hill, New York, 1984.

[34] Stanley Whitley, Rev. Mod. Phys. **56**, 41 (1984).

[35] P.A.M. Dirac, unpublished manuscript cited in K. Cohen, *Theory of Isotope Separation as Applied to the Large-scale Production of* ^{235}U, McGraw-Hill, New York, 1951.

[36] Stanley Whitley, Rev. Mod. Phys. **56**, 62 (1984).

[37] David J. Rose and Melville Clark, Jr., *Plasma and Controlled Fusion* M.I.T. Press, Cambridge, 1961.

[38] E.M. Little, W.E. Quinn, F.L. Ribe, and G.A. Sawyer, Nuc. Fusion Suppl. **2**, 497 (1962).

[39] H.R. Griem, *Plasma Spectroscopy*, McGraw-Hill, New York, 1964.

[40] Lymon Spitzer, Jr., *Physics of Fully Ionized Gases*, Interscience Publishers, New York, 1962.

[41] W.B. Herrmannsfeldt, Electron Trajectory Program, SLAC 226, Stanford Linear Accelerator Center, Stanford, CA 94305, November 1979.